Digital Fuel Control for a Lean Premixed Hydrogen-Fueled Gas Turbine Engine

Daniel C. Villarreal

Thesis submitted to the faculty of the
Virginia Polytechnic Institute and State University
in partial fulfillment of the requirements for the degree of

Master of Science
In
Mechanical Engineering

Committee Members
Walter F. O'Brien, Chair
Uri Vandsburger
Martin Johnson

August 28, 2009
Blacksburg, Virginia

Keywords: Gas Turbine Control, Hydrogen, Lean Premixed Combustion, Flashback, System Identification

Digital Fuel Control for a Lean Premixed Hydrogen-Fueled Gas Turbine Engine

Daniel C. Villarreal

(Abstract)

Hydrogen-powered engines have been gaining increasing interest due to the global concerns of the effects of hydrocarbon combustion on climate change. Gas turbines are suitable for operation on hydrogen fuel. This thesis reports the results of investigations of the special requirements of the fuel controller for a hydrogen gas turbine. In this investigation, a digital fuel controller for a hydrogen-fueled modified Pratt and Whitney PT6A-20 turboprop engine was successfully designed and implemented. Included in the design are safety measures to protect the operating personnel and the engine. A redundant fuel control is part of the final design to provide a second method of managing the engine should there be a malfunction in any part of the primary controller.

Parallel to this study, an investigation of the existing hydrogen combustor design was performed to analyze the upper stability limits that were restricting the operability of the engine. The upstream propagation of the flame into the premixer, more commonly known as a flashback, routinely occurred at 150 shaft horsepower during engine testing. The procedures for protecting the engine from a flashback were automated within the fuel controller, significantly reducing the response time from the previous (manual) method. Additionally, protection measures were added to ensure the inter-turbine temperature of the engine did not exceed published limits. Automatic engine starting and shutdown procedures were also added to the control logic, minimizing the effort needed by the operator. The tested performance of the engine with each of the control functions demonstrated the capability of the controller.

Methods to generate an engine-specific fuel control map were also studied. The control map would not only takes into account the operability limits of the engine, but also the stability limits of the premixing devices. Such a map is integral in the complete design of the engine fuel controller.

Acknowledgements

I would first like to thank my advisor Dr. O'Brien for giving me the opportunity to be a part of the Hydrogen project. I have always been a fan of challenges, and this certainly has been one of the biggest challenges that I have had here at Virginia Tech. Of course the project would not be possible without the support of our sponsors, Bruce Cambata and Dr. Joe Garst of Electric Jet, LLC. The enthusiasm they brought to our Monday meetings always kept me excited to continue progress on the fuel controller until completion. In addition, I would like to thank Dr. Vandsburger and Dr. Johnson for their insight and for their time spent helping me on this project.

Of course I could not have made it this far without the input and experiences shared with members of the Turbo Lab. Matt Perry has been a wonderful friend these two years and a great resource for sharing ideas. His expertise in gas turbine engines and his suggestions for helping me through my part of the Hydrogen project are deeply appreciated. Cape Thompson always brought life to the lab, even on the bad days when everyone felt locked down with work. Cape's attitude and life stories were a great distraction during the day. While only an unofficial member of the Turbo Lab, "Dr." Jordan Farina equally deserves to be mentioned. His childhood stories of the south have a tendency to bring myself and anyone nearby to their knees in laughter.

Other members of the Hydrogen project and the Turbo Lab also found their way to help get me going whenever I reached a roadblock. "Rescue" Steve LePera was (almost) always there to help me and the team out. Steve's input and experience helped immensely with this project. Additionally, the mathematical and programming expertise of both Bill Schneck and Chris Martin definitely helped just as it was needed. I would also like to thank Bill Hook helping me learn different aspects of the PT6 using hands on experience. His practical knowledge of gas turbine engines helped us come up with realistic methods for implementing some of our crazy ideas.

Finally, I want to thank my family and especially my friends for supporting me through the past two years, as well as providing me with welcome distractions. I think I might have gone crazy if I did not have a good bike ride, run, or nighttime adventure with some of my good friends that remained at Virginia Tech after my 2007 graduation. The experiences and memories I have of Blacksburg will stay with me forever.

Table of Contents

List of Figures

List of Tables

Notation and Abbreviations

$\boldsymbol{A}$	vector of signal amplitudes
c_{p_a}	specific heat of air
$c_{p_{f-a}}$	specific heat of fuel-air mixture
f	fuel – air ratio
f_0	fundamental frequency
G_{uy}, G_{yu}	cross spectra of input and output signal
G_{uu}	auto spectrum of input signal
G_{yy}	auto spectrum of output signal
h	impulse response
$\boldsymbol{i}$	vector of harmonic integers
J	polar moment of inertia
k	sample number
K_{cr}	critical proportional gain
K_d	derivative gain
K_i	integral gain
K_p	proportional gain
M	Mach number
$\dot{m}_a$	air mass flowrate
$\dot{m}_f$	fuel mass flowrate
n	compressor shaft speed, signal noise
N_2	compressor rotor speed
N_g	gas generator speed
N_p	output shaft speed
NO_x	oxides of Nitrogen
P_{02}	total pressure at compressor inlet
P_{03}	total pressure at compressor exit
P_{04}	total pressure at turbine inlet
P_{atm}	atmospheric pressure
P_b	burner pressure
P_{cr}	critical period of oscillation
$\mathcal{P}$	shaft power output
$\mathcal{P}_c$	compressor power
$\mathcal{P}_t$	turbine power
Q_R	heat of reaction
T_{atm}	atmospheric temperature
T_{02}	total temperature at compressor inlet
T_{04}	total temperature at turbine inlet
T_4	turbine inlet temperature
T_d	derivative time
T_i	integral time
T_s	sampling interval
$\mathcal{T}$	torque
u	input signal
$\boldsymbol{U}$	control vector
$\boldsymbol{V}$	atmospheric conditions vector
V_{DC}	DC voltage
$\boldsymbol{X}$	state vector
y	output signal
$\hat{y}$	output signal without noise
$\boldsymbol{Y}$	output vector
η_t	turbine efficiency
θ	corrected temperature
$\boldsymbol{\phi}$	vector of phases

A/D	Analog/Digital
DAQ	Data Acquisition
DEBB	Digital Electronic BreadBoard
EEC	Electronic Engine Control
FADEC	Full Authority Digital Electronic Control
FFT	Fast Fourier Transform
FRF	Frequency Response Function
HMC	Hydro-Mechanical Control
ITT	Inter-Turbine Temperature
LPR	Low Pressure Regulator
PDF	Pseudo-Derivative Feedback
PID	Proportional-Integral-Derivative
SCF	Standard Cubic Feet
SFC	Specific Fuel Consumption
SNR	Signal-to-Noise Ratio
SPDT	Single-Pole Double-Throw
SPST	Single-Pole Single-Throw
TC	ThermoCouple
UPS	Uninterruptible Power Supply
VI	Virtual Instrument
ZOH	Zero-Order Hold

Chapter 1: Introduction

1.1 Background and Motivation

Hydrogen fuel in aero propulsion and power generation has been gaining interest due to the recent push toward alternative sources of energy. It is viewed as an attractive substitute to hydrocarbon fuels because not only does it have the potential to reduce the world's dependence on fossil fuels, it also has the capability to drastically reduce the emissions that are currently created from hydrocarbon fuel combustion. While current gas turbine engines have had decades of evolution to improve fuel efficiencies, there is a growing desire to find a feasible alternative fuel, with hydrogen being appealing because of its chemical properties and zero carbon emissions.

As a part of the research currently being performed on hydrogen-fueled gas turbines, control methods also must be established to maintain a level of operability similar to those of existing engines. Fuel control is dependent on the dynamics of the engine, and a proper fuel schedule should protect the engine from exceeding its operability limits. The following material emphasizes considerations for control of hydrogen gas turbine engines with emphasis on the aircraft application. However, the discussions and the results are generally applicable to both aircraft and stationary gas turbines.

1.1.1 Emissions

Existing aircraft gas turbine engines burn hydrocarbon fuels and produce a variety of pollutants during operation. These pollutants include, but are not limited to, carbon dioxide (CO_2), carbon monoxide (CO), oxides of nitrogen (NO_x), oxides of sulphur (SO_x), water vapor, and unburned hydrocarbons [1]. Hydrogen combustion, however, has emissions that are limited to water vapor

and NO_x. Water vapor has the potential to affect ozone production above a certain altitude, but these effects have been considered negligible when compared to natural occurrences [2]. NO_x is a combination of nitric oxide (NO), nitrous oxide (N_2O), and nitrogen dioxide (NO_2) and is a source of smog and acid rain. It is mainly produced from the thermal formation of NO and prompt-NO which is formed in the flame zone, as described by the Zeldovich and Fenimore mechanisms, respectively. Thermal NO_x formation has been shown to be highly dependent on temperature and residence time [1][3].

The formation of NO_x can be reduced by premixing hydrogen with air prior to combustion. Hydrogen has a much wider flammability range than that of conventional aircraft fuels, with equivalence ratios ranging between 0.12 and 6.10 [4]. This range allows for combustion at much leaner equivalence ratios than that of kerosene, potentially reducing the NO_x formation as a result of the lower flame temperatures. The lean blowout limits of hydrogen and kerosene are shown in Figure 1.1 [5].

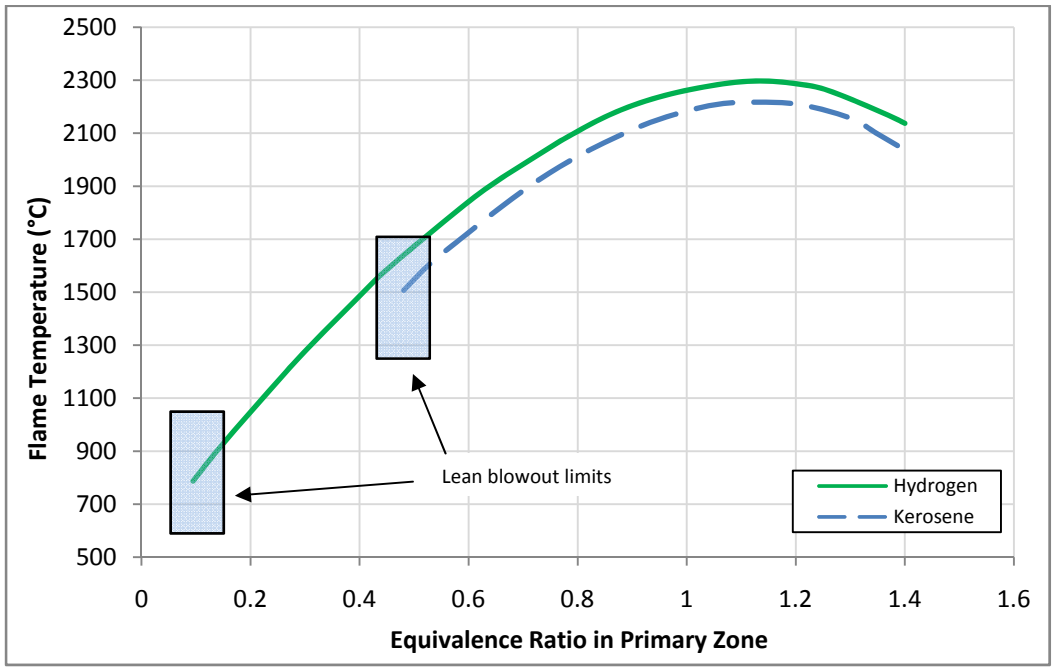

Figure 1.1. Theoretical flame temperature as a function of equivalence ratio for hydrogen and kerosene (Courtesy AIAA) [5]

1.1.2 Flame Stability Limits

Flame stabilization of lean-premixed hydrogen becomes a concern at lower equivalence ratios. The velocity of the combustible mixture has to be high enough to prevent the flame from propagating upstream into the premixing device (or simply premixer) [1]. The upstream flame propagation, known as a flashback, can damage the engine and premixers and can be detrimental to engine performance. However, flame lifting and blowout can occur if the velocity of the mixture is too high for the flame to remain attached to its flame holder [1].

1.1.3 Hydrogen Storage

Hydrogen is also an appealing alternative fuel because of its high heat of combustion, high specific heat, and low density [2]. The lower heating value of hydrogen is approximately 2.8 times that of Jet-A, resulting in a fuel weight requirement considerably less for hydrogen aircraft structures. In addition, the high specific heat of hydrogen allows for engine cooling prior to combustion as well as lower specific fuel consumption (SFC). However, due to the low density of hydrogen, more fuel volume is required for the equivalent energy of Jet-A. A solution to this problem is to cryogenically store the hydrogen to maximize the amount of fuel in a storage tank, though this leads to other engine and aircraft design issues that are not addressed in this thesis. Table 1.1 summarizes some physical properties for hydrogen and Jet-A aircraft fuel.

Table 1.1. Comparison of physical properties of hydrogen and Jet-A [2]

	Hydrogen	**Jet-A**
Lower heating value kJ/g (Btu/lb)	120 (51,590)	42.8 (18,400)
Specific heat J/g-K (Btu/lb-^{o}F)	9.69 (2.32)	1.98 (0.47)
Liquid density at 283 K g/cm^3 (lb/ft^3)	0.071 (4.43)	0.811 (50.6)

1.2 Control Methods

As hydrogen gas turbine engine technology evolves, so do the fuel systems and associated control methods for passing hydrogen through the supply lines to the combustion chamber. Emission levels can be improved passively by burning hydrogen using a lean-premixed approach, as is the case in this investigation; however, there are flame stability concerns that

must be addressed with this combustion method, most notably those of flashback and flame blowout. To protect the engine from these instabilities, an engine fuel controller has to be able to automatically take corrective actions to prevent engine damage. The fuel system must also be able to safely transfer hydrogen from its source to the combustion chamber with redundant modes of operation.

1.3 Current Work

The focus of the current work is the control of gaseous hydrogen through a fuel supply system to power a modified Pratt and Whitney Canada PT6A-20 turboprop engine rated to 550 shaft horsepower. The combustor of the PT6A-20 has been redesigned to operate using hydrogen fuel-air premixers and a matching combustor liner to allow for lean premixed hydrogen combustion. A data acquisition system has been coupled to the fuel control system and engine to allow for real-time measurements, with some measurements being used as control feedback. The fuel is regulated to the engine through an electronically controlled pressure regulator that is managed by a computer.

Early engine testing with the hydrogen-air premixers showed that flashbacks occurred under specific engine conditions. As a result, the fuel controller was designed to monitor the premixer shell temperatures for sudden jumps, indicating a flashback. In the event of a flashback, the controller performs a series of actions to prevent damage to the engine. Other safety precautions were also included in the control logic to protect both the engine and operating personnel. The performance of the fuel controller and engine were analyzed during each step of fuel control development.

This thesis presents in detail the design of the fuel controller. *Chapter 2* is a review of literature related to fuel control methods and hydrogen combustion in gas turbine engines. The design and construction, control logic, and performance of the fuel controller and engine are presented in *Chapters 3-5*. Next, approaches to creating analytical and experimental models to be incorporated into the fuel controller are summarized. The fuel control map for the engine was unavailable for this investigation, so experiments using the new fuel controller were carried out in a conservative manner to avoid high turbine inlet temperatures, engine surge, and premixer

flashback. Implementing methods for experimentally determining a control map is discussed in *Chapter 6*. Finally, this work concludes with *Chapter 7* which summarizes the fuel control design and performance and presents recommendations to improve its performance.

Chapter 2: Review of Literature

This chapter presents past work related to gas turbine propulsion control technology and the studies performed on the combustion of hydrogen in a gas turbine engine. It begins with the evolution of gas turbine fuel control, from hydromechanical controllers to FADEC systems. This section is followed by reviewing engine tests in which hydrogen fuel was burned using diffusion flames. Finally, different hydrogen control methods used during engine tests are summarized.

2.1 Gas Turbine Fuel Control

The need for fuel controls for gas turbine propulsion engines has existed since the 1940s, with control technology becoming more sophisticated as propulsion technology became more advanced. Gas turbine engine fuel control has evolved from mechanical speed governors and hydro-mechanical controls (HMC) that managed no more than three engine variables, to modern aircraft control systems that use sensors located throughout the engine as feedback in full authority digital electronic controllers (FADEC). These electronic control systems manage all engine functions and are fully redundant, eliminating the need for HMC backup. Today, complex FADEC systems for military aircraft can simultaneously control more than ten engine variables.

In its simplest form, an engine fuel control system supplies the fuel needed to achieve an engine power demand. Since the 1970s, digital feedback has become more integral to the fuel control system [6]. Modern control systems can calculate commands based on sensor feedback and adjust actuator and valve settings up to 80 times per second [7]. A simplified schematic of an

electronic fuel controller is shown in Figure 2.1. An operator requests the power or thrust from the engine by changing the throttle or power lever angle and the fuel is supplied according to a fuel schedule that is dependent on the operating limits of the turbomachinery. The fuel schedule and operating limits are usually determined at the time of engine development. Measurements of inlet temperature and inlet pressure are used to calculate aircraft altitude and Mach number as well as to compute corrected data based on sea level standard conditions [8].

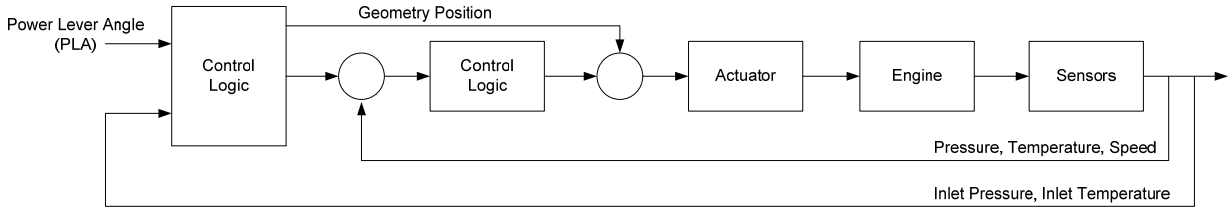

Figure 2.1. Simplified digital electronic engine control system schematic [7]

Rajagopalan,et al., of Pratt and Whitney provided an overview of the history of propulsion controls and engine health monitoring [6]. During the 1970s, Pratt and Whitney developed a digital electronic bread board (DEBB) to evaluate and develop cam schedules used in the F100 hydromechanical control. Electronics in this application allowed investigators to realize that computers could reduce both electronic control and engine development cycle time, leading to a transition of the F100 hydromechanical controls to electronic engine control (EEC). Requirements of the EEC for minimal pilot attention included [9]:

1. Simple starting procedures without the need for simultaneous actuation of switches
2. Unrestricted power lever movements
3. Rapid thrust transient capability free of surge or blowout
4. Engine protection during start-up and operation

With EEC used in a supervisory manner, the pilot could request a power or thrust and the computer calculated and regulated the fuel flow required to maintain that setting. However, since electronics technology at the advent of EEC had low dependability, hydromechanical backups were still implemented with separate engine diagnostic units in the event of EEC malfunction. The backup HMC had conservative, fixed fuel-ratio maximum and minimum

schedules [10]. A full authority digital EEC (FADEC) evolved from the supervisory EEC and DEBB and was first flight tested with the F100 in 1981. FADEC systems have since become more sophisticated with the evolution of propulsion technology. Figure 2.2 shows the trends in engine control complexity in military and commercial application from 1940 to 2000.

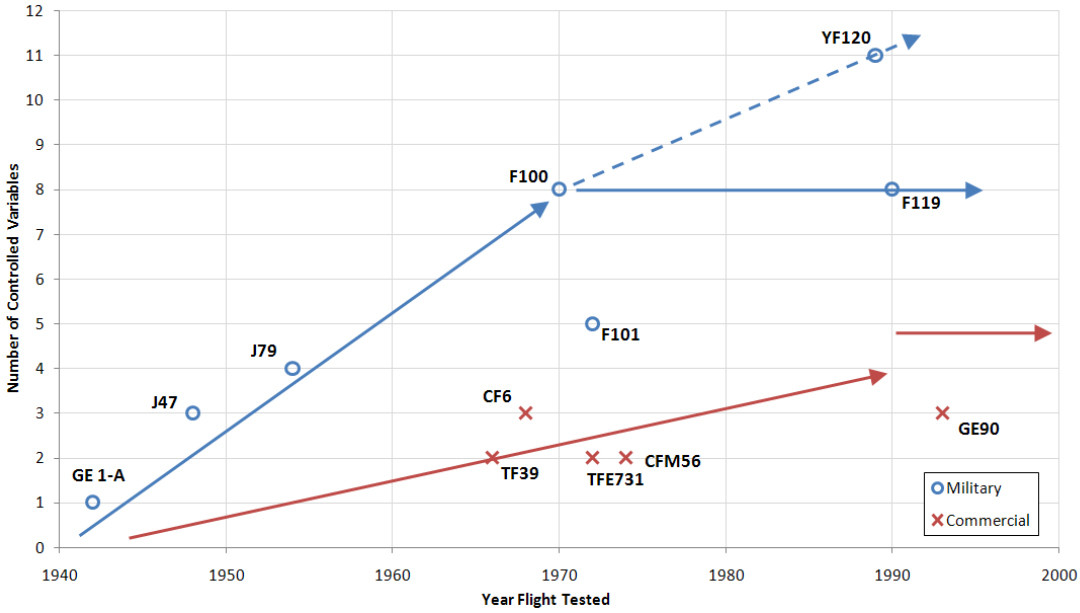

Figure 2.2. Trends of engine control complexity in military and commercial engines [10]

Computer-controlled fuel systems follow a control map in order to avoid prohibited operating points of the engine that could lead to high turbine inlet temperatures (inter-turbine or exhaust gas temperatures), compressor overspeed, or compressor surge. A control map, or fuel schedule, for a dual-spool engine is shown in Figure 2.3 where $\dot{m}_f$ is the fuel flow rate, P_b is the burner pressure, and N_2 is the rotor speed [11]. The fuel schedule depicts the safe operating limits of the engine and is unique to each type of gas turbine engine. The maximum rate of acceleration to avoid compressor surge is shown as the upper limit. A limit on deceleration rate prevents flame out (blowout) or total loss of combustion. The right-most limit represents the maximum temperature that the compressor can manage before the turbine disc begins to creep. A safety margin for disc creep is implemented through the use of the maximum governor. The area between the idle and maximum governors and between the acceleration and deceleration limits is

the range of operation of the gas turbine engine. Models of the fuel schedule are incorporated into the fuel controller to provide the most appropriate engine response without infringing on any of the limits shown. In most cases, the fuel schedule is dependent on the turbine gas temperatures because of the range of temperatures the turbine can encounter. Manufacturers often create a temperature schedule for the turbine that is used in the control map development.

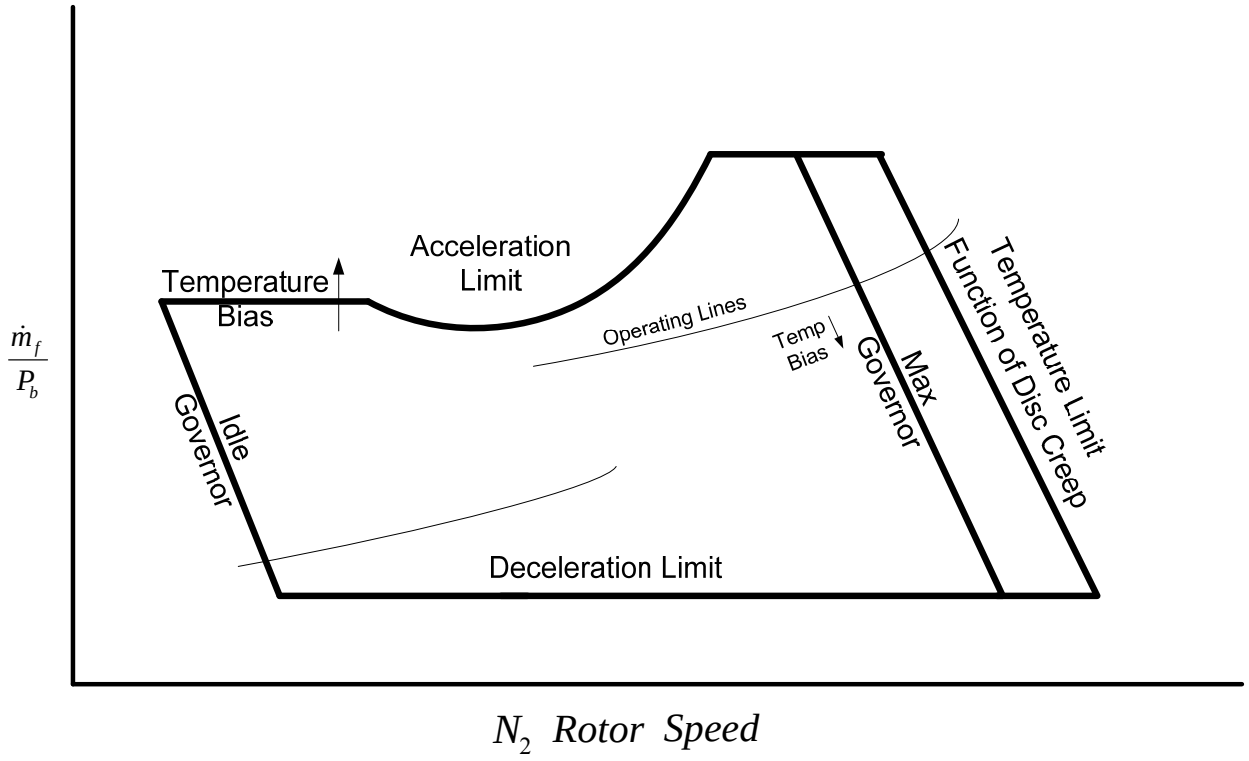

Figure 2.3. Control map depicting operating limits of a gas turbine engine [11]

Model-based control has become increasingly important in the development of propulsion fuel control technology. A block diagram of model-based control architecture is shown in Figure 2.4. During engine development, a nonlinear model of the engine is created that is used in the controller design [7]. The model is simplified through linearization and compared to the original to ensure the response characteristics are the same. Control design begins when the model is considered acceptable. The controller feeds commands into the model and the response can be analyzed to determine if controller design changes are necessary before installation with the

physical engine. The model is embedded into the control logic to provide a means for direct control of thrust and engine limits.

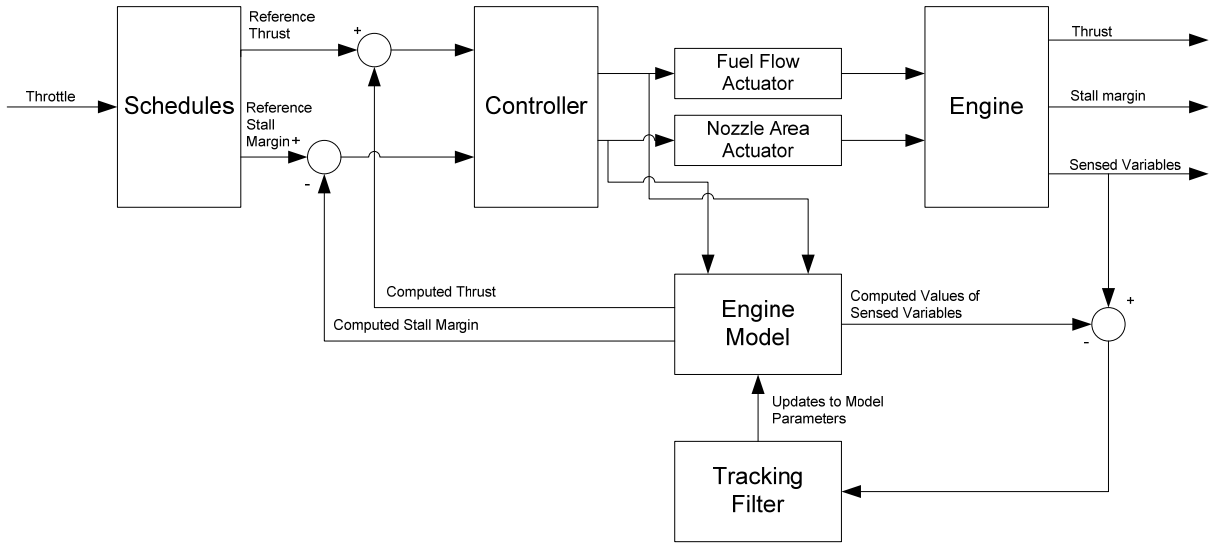

Figure 2.4. Model-based control architecture [7]

The engine model can be tuned using a tracking filter to account for variations between engines, engine deterioration, and even modeling errors. The tracking filter matches the model to the engine by adjusting the model's inputs and parameters, creating a more accurate representation of the engine. Different engine models (operability, performance, diagnostics, acoustics, etc.) require separate tracking filters. Development of a method for matching all models simultaneously has been challenging due to memory and processing limitations of current FADECs [7][12]. Processor evolution for propulsion control has not kept pace with the introduction of new high performance processors due to several selection factors. This is especially true when the processors are considered for military applications. Selection factors include processor speed, cost, obsolescence, programmability, and temperature/vibration requirements [6].

Multi-core processors are currently being explored as the next step in engine control evolution. These processors would allow simultaneous control mode calculations based on measurement feedback analysis. Shown in Figure 2.5 is a possible multi-core processor distribution of FADEC functions that could be used in future engine control designs [13]. After installation, a

FADEC using a multi-core processor could be updated with new functions using previously unused processors.

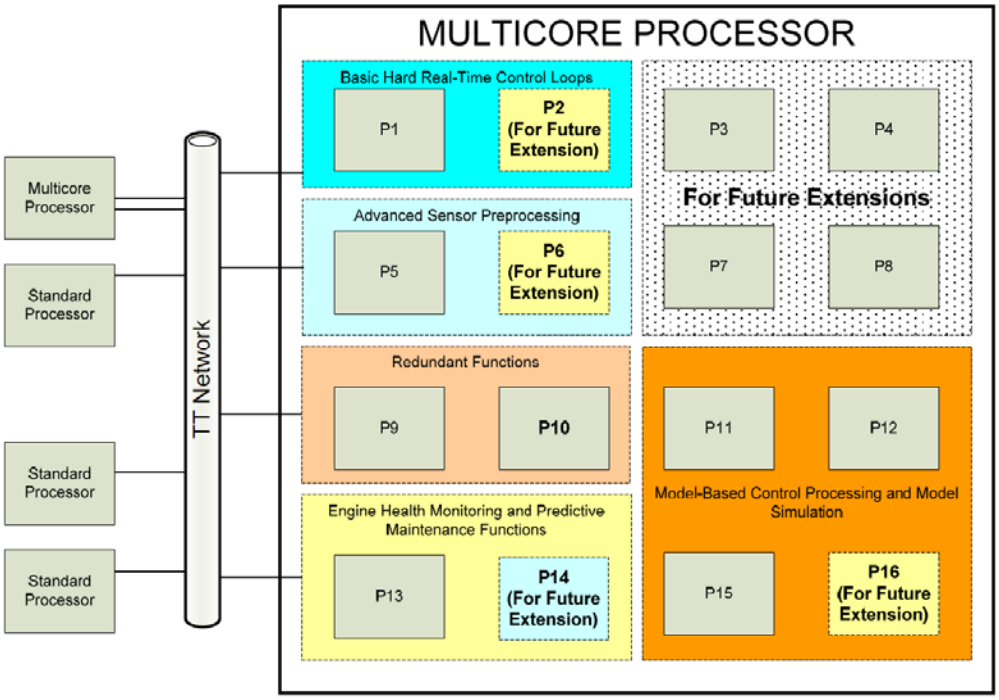

Figure 2.5. Hypothetical distribution of FADEC functions on a multi-core processor [13]

2.2 Hydrogen-Fueled Gas Turbines

In the book *Hydrogen Aircraft Technology*, Brewer describes early experimental work with hydrogen combustion for gas turbine aircraft propulsion [2]. A 1956 NACA-Lewis flight test of a B-57 twin-engine medium bomber demonstrated the feasibility of burning hydrogen in a turbojet at high altitude. Hydrogen in these experiments was burned in a diffusion manner. The engines used were two J-65 turbojet engines, with one having modifications for hydrogen combustion. In the experiments, the B-57 took off using conventional JP jet fuel in both engines and accelerated to the test altitude and speed (usually 50,000 ft and Mach 0.75), at which time the JP fuel of the test engine was reduced and stopped while gaseous hydrogen was introduced until it reached the required flowrate. After completion of the flight test, JP fuel was re-introduced to the test engine and the aircraft descended and landed.

Also in 1956, Pratt and Whitney was awarded a U.S. Air Force contract to investigate the feasibility of modifying existing gas turbine engines to operate on hydrogen [14]. Pratt and Whitney began investigations by converting a J57 turbojet engine to operate on liquid hydrogen fuel. With knowledge gained from initial testing of the J57, Pratt and Whitney designed, built, and tested a new engine designated the Model 304 that operated on liquid hydrogen. Over 25 hours of testing were performed on the engines from 1956 to 1958. The engine was capable of producing 12,000 lbs of thrust with a hydrogen flow rate of 4 lb/s (1.8 kg/s). Two liquid hydrogen-fueled Model 304 engines were to be used in the Lockheed CL-400 aircraft designed for reconnaissance missions, however the project ended in 1959 and flight tests were never conducted.

In 1988 Sosounov and Orlov performed a flight test of a Tupolev-155 three-engine passenger aircraft in which one of the three Kuznetsov NK-88 turbofan engines was converted to burn liquid hydrogen [15]. In this system, liquid hydrogen was supplied by a turbine-driven fuel pump and ran through a heat exchanger before reaching the combustion chamber. The problems encountered with this fuel supply system included the simultaneous development of the fuel pump, turbine, heat exchanger, and the fuel control associated with the fuel pump. For the flight test, the hydrogen-powered engine was operational during take-off, cruise, and landing. In the event of a hydrogen leak, nitrogen could be used to fill the fuel tank section of the aircraft or it could be constantly purged using air that was bled from the engine compressor.

2.3 Challenges of H_2 Control for Propulsion

The design of a hydrogen propulsion system has been considered a challenge due to hydrogen's low density and wide flammability range. In 2003, Brand, et al., described some of the design requirements that should be considered when burning hydrogen in a gas turbine aircraft engine [5]. For the conversion of a hydrocarbon-fueled engine, the authors stated that changes include modification to the fuel supply and control system, the combustion system, and additions of a hydrogen purge system and hydrogen leak indication system.

In 1975, a United Aircraft of Canada Ltd (now Pratt and Whitney Canada) ST6-68 gas turbine engine was converted to hydrogen combustion and successfully powered a 36-foot landing craft [16]. The ST6 engine was rated to 350 shaft horsepower and was capable accelerating the

landing craft to 30 knots in calm water. The original combustor liner was replaced with one that allowed more dilution air and the kerosene fuel nozzles were modified for hydrogen diffusion combustion. Forty-eight commercial gas cylinders were manifolded together to supply the engine with 21.3 kg (12,000 SCF) of hydrogen. Several valves in the fuel supply line were designed to be failsafe closed in the event of an emergency. As part of normal operating procedures, a nitrogen purge was performed on the system to clear the fuel lines of hydrogen before and after engine operation. This project showed that modifications to the engine for hydrogen operation affected both the fuel controls and combustor design (liner and fuel nozzles).

Care was taken to ensure that fuel-air premixers were properly staged and controlled in a study of NO_x formation in a hydrogen-fueled microturbine [17]. Therkelsen, et al., looked at different injection schemes and corresponding engine performance and emissions levels. The test engine was a 60 kW Capstone C60 natural gas microturbine designed with fuel-air premixers. In each experiment, pilot hydrogen premixers were always fueled during engine operation while fuel in the remaining premixers was varied according to engine power request. The fuel control system was based on feedback signals of exhaust temperatures and engine shaft speed. The data acquisition system provided engine operational data that included power output, shaft speed, air and fuel flow rates, fuel pressures, and ambient temperatures.

2.4 Summary

This section summarized the evolution of fuel controls in aircraft gas turbine propulsion, from hydromechanical controls to electronically redundant FADEC systems. Early electronic controls had HMC backup control due to the low reliability of the emerging technology, but when the electronic systems proved to be more capable and reliable than their hydromechanical counterparts, the controllers were transitioned to fully electronic systems. Hydrogen combustion in gas turbine engines was also been summarized, with flight experiments as early as the 1950s. However, the experiments discussed in this thesis were primarily concerned with determining the feasibility of converting an existing engine to one that could operate on hydrogen using diffusion combustion. When considering engine performance and emissions reduction, more design is required for both the engine combustor and control system.

Chapter 3: Control System Design and Construction

The development of the fuel controller occurred during the same time that a study on the characteristics of the hydrogen-air premixers was being performed. Two premixer-combustor liner designs were tested in the engine to improve its operating limits, with the controller demonstrating its versatility to quickly be adapted and perform equally the same for both designs. This chapter details the design and construction of the fuel controller with the most recent premixer design.

3.1 Gas Turbine Setup

The test engine was a modified Pratt and Whitney Canada PT6A-20 turboprop rated at 550 shaft horsepower. A photograph of the engine test setup is shown in Figure 3.1 with a schematic shown in Figure 3.2. The engine sits on a test stand and uses a water-brake dynamometer with PID control to vary the load on the output shaft in order to control its speed at a predetermined setting. The dynamometer is capable of dissipating up to 1,000 horsepower. The torque applied to the output shaft is measured and used with shaft speed to calculate engine power output. For all tests, the shaft speed was held constant at 2000 rpm.

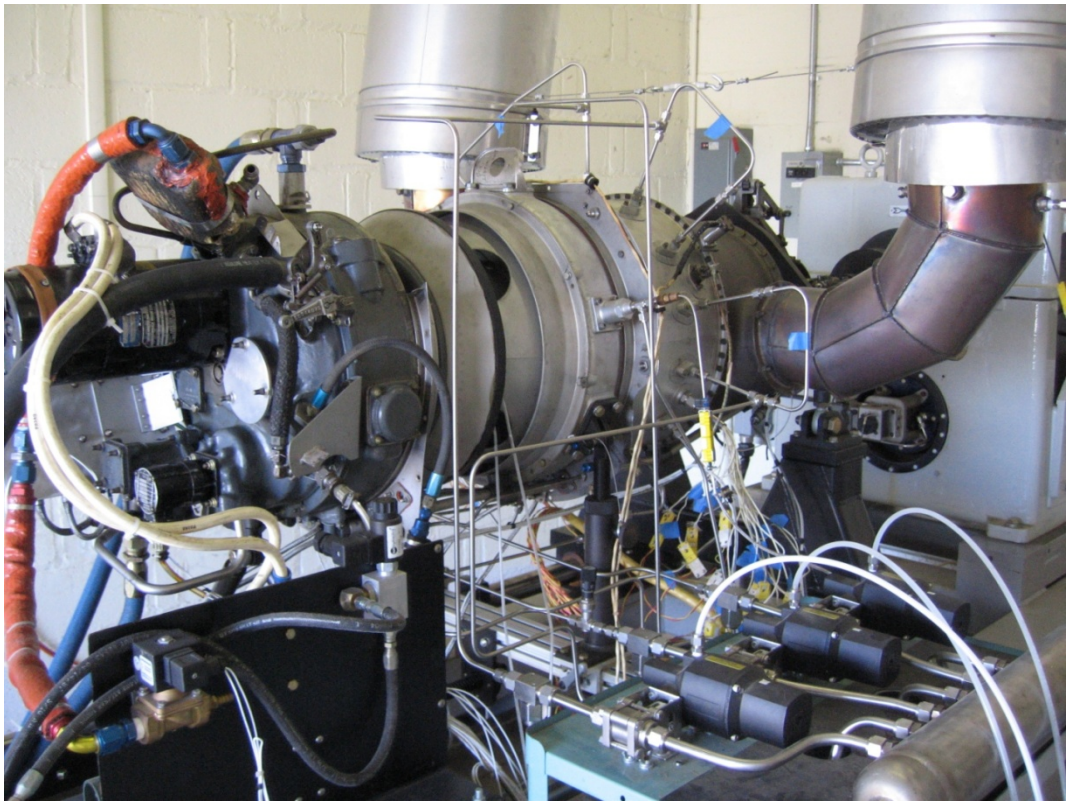

Figure 3.1. PT6A-20 turboprop engine, test stand, and hydrogen supply valves

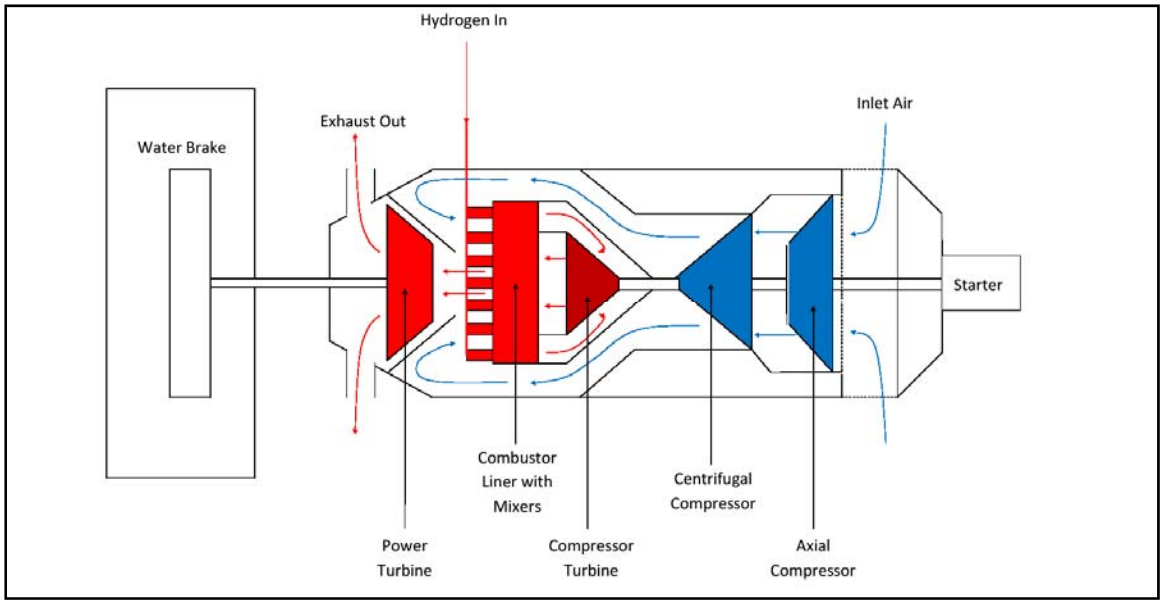

Figure 3.2. Engine schematic showing installation of premixers and liner [18]

The combustion chamber design contained 14 or 18 hydrogen-air premixers that were evenly spaced in a custom-designed combustor liner. During engine development, combustor designs with 14 and 18 premixers were tested, with the 14 premixer design ultimately selected. The controller was adapted to the number of premixers utilized in a given test, with no effect on the basic design of the controller. The premixers had choked fuel ports to eliminate the chance of combustion instabilities coupling to the fuel supply [19]. Temperatures of the premixers were monitored using thermocouples that were attached to the shell of the premixer. A photograph of the modified combustion chamber with 14 premixers is shown in Figure 3.3a. The premixers were arranged in six banks to allow for automatic staged starting and for closing of individual banks in the event of a flashback. A schematic of the premixer bank arrangement and locations of the thermocouples (TC) and T_4 probes is shown in Figure 3.3b. The numbering scheme shown was used in the flashback control logic, which is described in the next chapter. Each bank was connected to a pneumatic ball valve that was actuated by energizing a solenoid valve located in the control room.

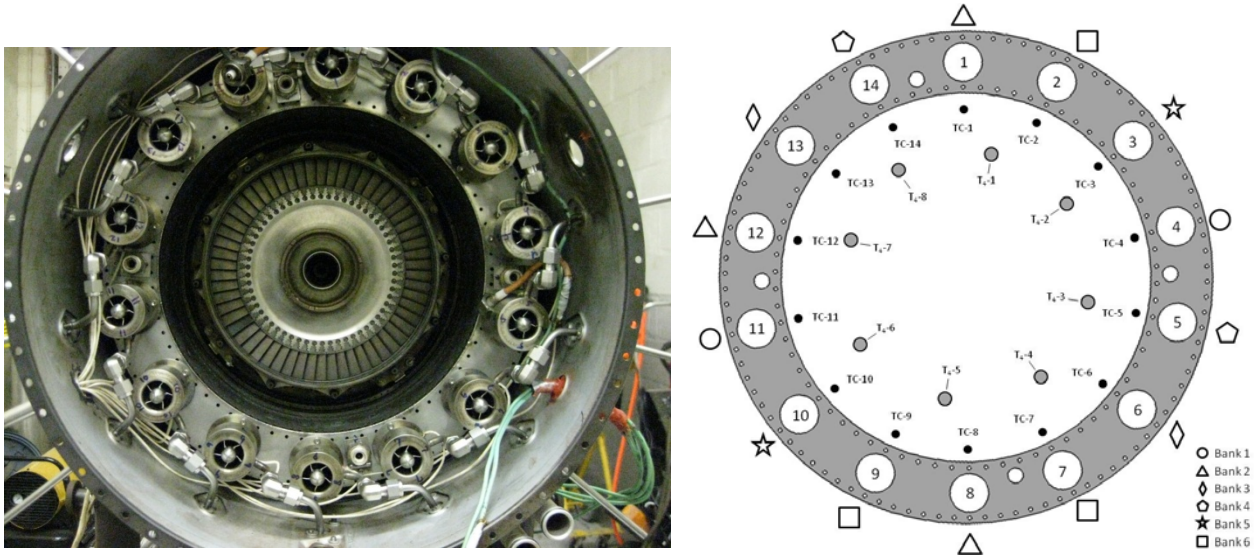

(a) (b)

Figure 3.3. (a) Combustion chamber with premixers and combustor liner installed, (b) premixer numbering scheme and bank arrangement

3.2 Hydrogen Fuel Supply System

The hydrogen fuel supply system consists of 316 stainless steel tubing with a series of pneumatically actuated ball valves to permit indirect control of the valve position. Stainless steel was chosen because of its strength and durability, resistance to oxidation, and low susceptibility to hydrogen embrittlement at high pressures [20]. Pressurized nitrogen at 110 psig was used for actuating each of the pneumatic valves, with controls located in a separate room from the engine. Pressurized dry air used with 40 micron filters could also be used for pneumatic valve actuation.

Following the simplified system diagram in Figure 3.4, hydrogen is supplied at 2300 psia to provide 3000 SCF of fuel. The pressure is reduced to 800 psig, corresponding to the system feed pressure. Located downstream of the pressure reducing regulator is a system pressure valve that allows the hydrogen to enter the fuel system. As with all the pneumatic ball valves in the system, the system pressure valve is opened and closed by energizing a solenoid valve from the control room. The fuel continues until it reaches the manifold valve that, once opened, provides the feed pressure to an electronically-controlled pressure regulator. Pressure regulation directly and proportionally controls the fuel flow into the engine due to the premixers' choked fuel ports. The pressure regulator is the primary means by which fuel is regulated to the engine to vary its power output. Downstream of the pressure regulator is a fuel manifold in which hydrogen is evenly dispersed into six separate lines corresponding to the banks of premixers.

The fuel lines can be bled of hydrogen by opening a bleed valve that is open to the atmosphere. The bleed valve is closed during normal operation. A purge valve, also closed during engine operation, can be opened to flow nitrogen through the fuel system. The fuel supply lines are cleared with nitrogen when both the purge valve and the bleed valves are open.

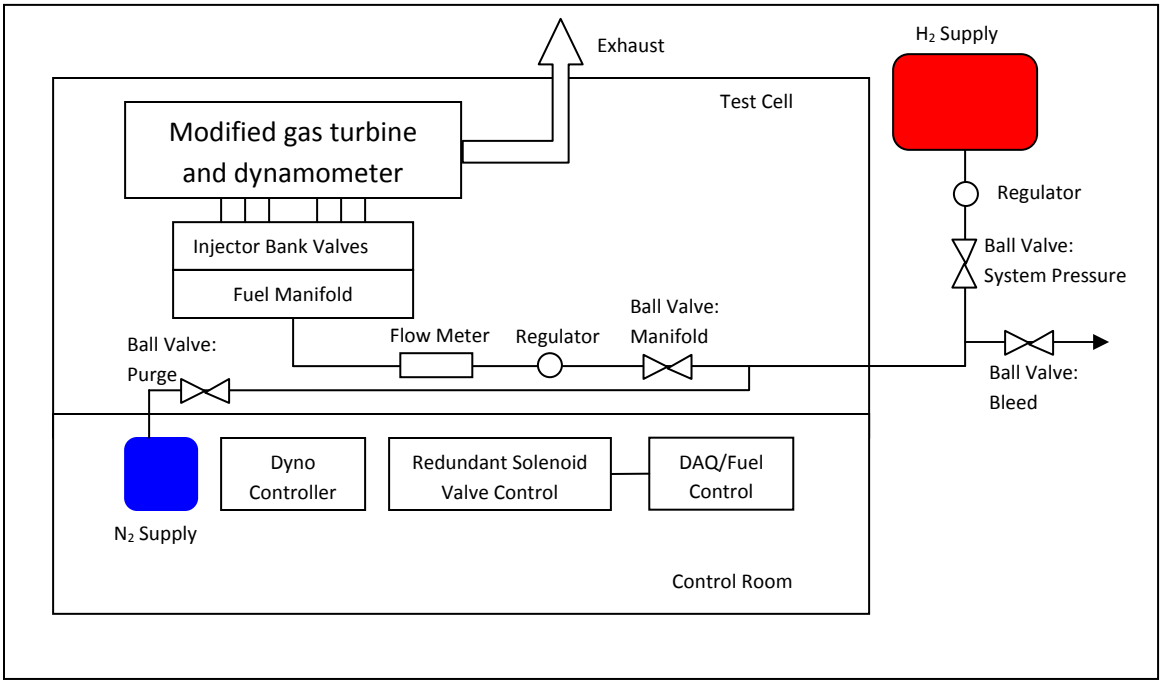

Figure 3.4. Hydrogen fuel supply diagram [18]

3.2.1 Pressure regulation

The pressure regulator is a Tescom ER3100 Series PID-controlled electronic regulator integrated with a Tescom 44-4000 Series dome-loaded pressure regulator. A picture of the integrated pressure regulator is shown in Figure 3.5a. During operation a protective cover is placed over the electronics, shown in Figure 3.5b. The ER3100 accepts pressure setpoints using either an analog input (4-20mA) or input through a digital RS485 computer interface [21]. The integrated system is capable of regulating a maximum 6000 psig inlet pressure down to a 50-1500 psig range. Pressure for the dome of the regulator is fed off the same lines as those for the pneumatic valves used throughout the fuel system. More detailed specifications of the ER3100 electronic controller and the 44-4000 pressure regulator are given in the appendix.

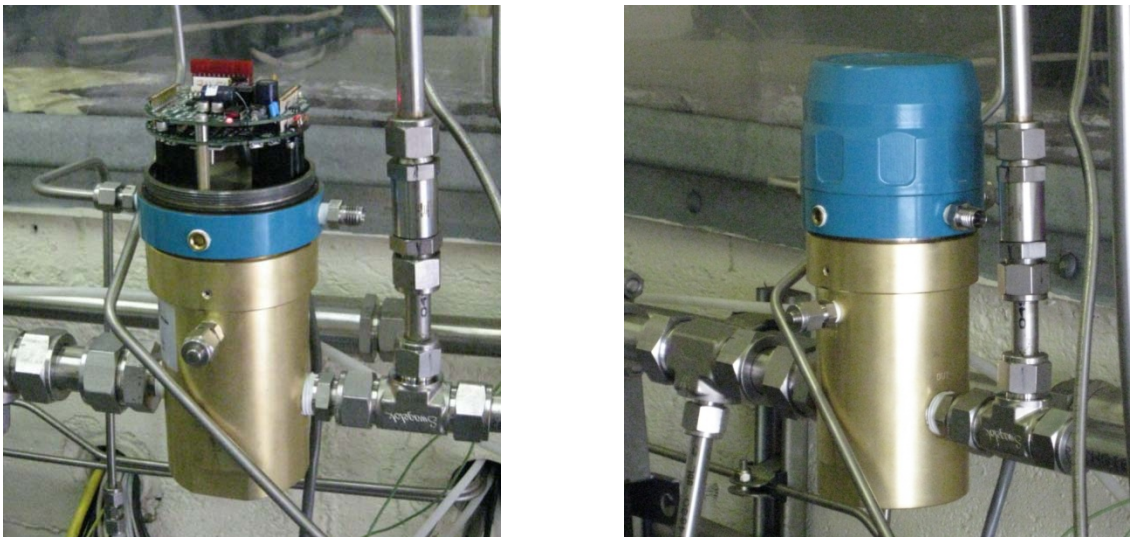

(a) (b)

Figure 3.5. Tescom ER3100 integrated electronic pressure controller (a) showing electronics and (b) with protective cover

3.2.2 Redundant fuel flow control

The actuating gas for the pneumatic valves can be either nitrogen or dry air. Pneumatic actuation is enabled by energizing 6-watt solenoid valves, connected so as to allow the fuel control system to have redundant control modes. The circuit diagram of this system is shown in Figure 3.6. A 300-watt power supply is used for energizing the solenoid valves as well as supplying the computer-controlled power. From the main voltage source, a master switch enables the voltage to reach single pole, single throw (SPST) switches that correspond to premixer bank (injector) "master" and system operation "master" switches. These SPST switches must be toggled to the 'ON' position for operation. The purpose of these switches is to de-energize solenoid valves in groups in the event of an emergency and return the pneumatic valves to their failsafe positions. Failsafe is a closed position for the individual premixer bank valves, the manifold valve, and the system pressure valve while the purge and bleed valves are failsafe open.

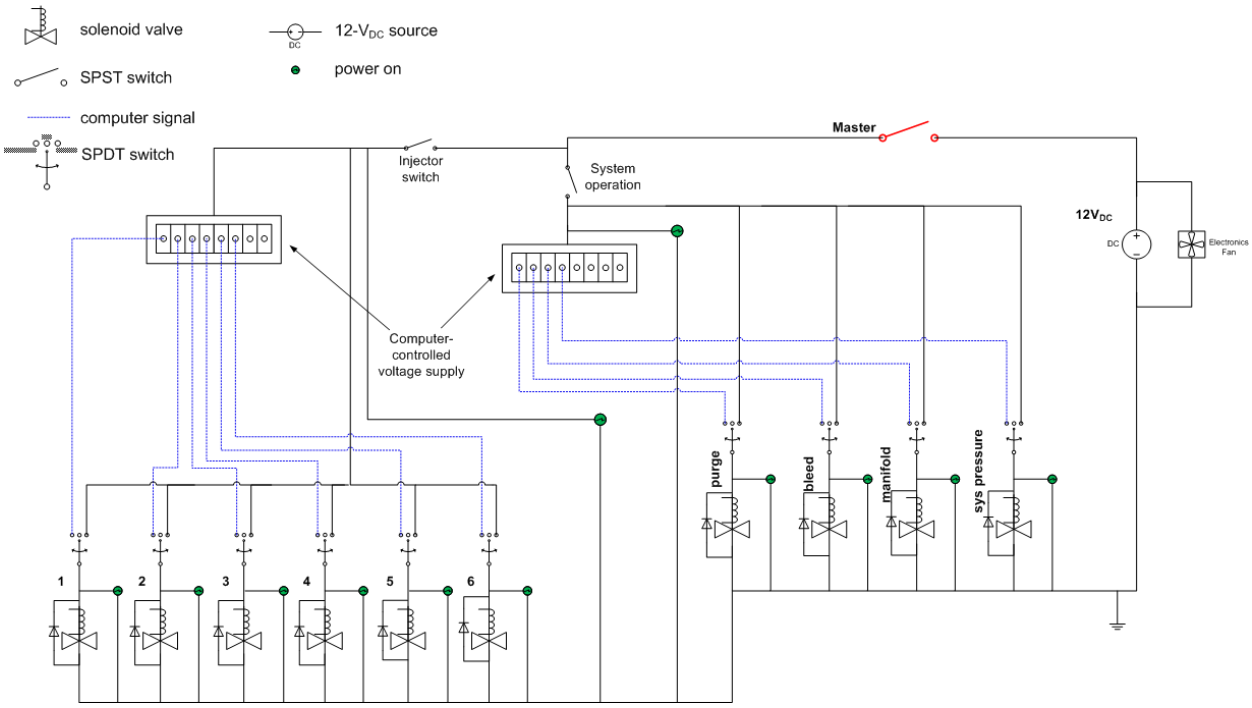

Figure 3.6. Circuit diagram showing the redundant control for energizing the solenoid valves.

With power available for the solenoid valves, the operator chooses solenoid control methods by using a single pole, double throw (SPDT) switch to toggle between a redundant "manual" and the primary computer control. The purpose of having a redundant manual control option is to provide a separate means of managing the pneumatic valves should the computer experience a malfunction. A picture of the constructed switch panel is shown in Figure 3.7. The diagram on the panel corresponds to the path that the hydrogen follows when the fuel supply has been opened, as well as the path that nitrogen takes during the purging process. For both control options, a green LED illuminates when its corresponding solenoid valve energizes, providing a visual representation of the position of the ball valves. In "manual" control the solenoid valves are energized independent of the computer. It was decided not integrate the CO_2 flood valve with the electronic system so that potential fires could still be suppressed in the event of a fire and loss of power.

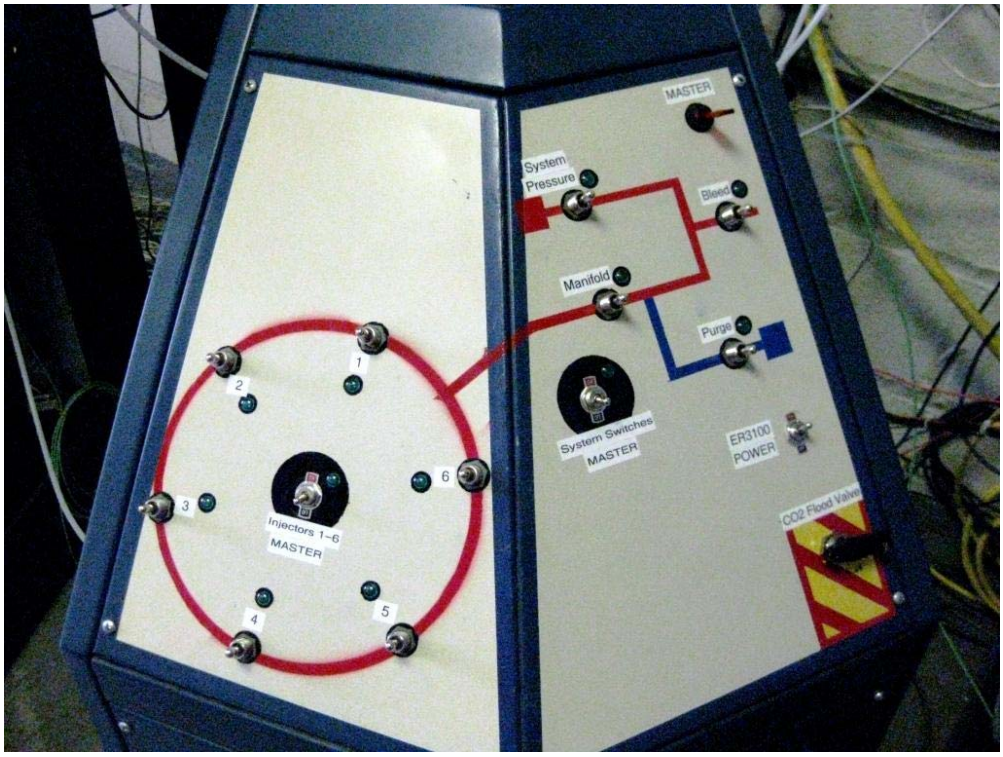

Figure 3.7. Solenoid valve physical control panel.

When the SPDT switch is set to computer control, the fuel controller programmed into the computer has the capability to manage operation of the solenoid valves. The computer interface has the same function as that of the physical panel, but allows for automatic control during different operation modes of the engine, including preparation for ignition (engine priming), transient operation, engine shut down, and fuel system purging. These functions are described in detail in the next chapter.

The control system power supply is connected to an APC 865-watt uninterruptible power supply (UPS) to allow continuous operation for a limited amount of time in the event of a power loss. The engine has the potential to be damaged should the fuel supply be cut off due to a loss of pneumatic pressure that causes the ball valves to return to their failsafe positions. The UPS gives the operator sufficient time to safely manage the fuel system and shut down the engine in a controlled manner.

3.3 Summary of Control System Construction

The control system was designed with safety as a primary concern, which dictated that the operator be distanced from the hydrogen fuel lines. Throughout the system are a series of pneumatic valves that, when in their normal operating position, allow hydrogen to flow from its source into the engine. The failsafe positions of the valves are such that the hydrogen is cut off from its supply and is prevented from entering engine. At the same time, hydrogen is purged from the fuel lines into the atmosphere.

Energized solenoid valves actuate the pneumatic valves, allowing for redundant control methods via operator or computer. The operator decides the control method by toggling the position of a SPDT switch associated with the valve. The redundant control is implemented in case there is a malfunction with the computer control, giving the operator a separate method for safely shutting down the engine.

Chapter 4: DAQ and Control Logic

This section describes the data acquisition and control systems used for controller and engine testing. The control system is broken down into two parts: one that describes the fuel control methods and one describing the automatic functions that occur during engine operation.

4.1 Data Acquisition

Real-time data from the engine and fuel system was acquired through a data acquisition (DAQ) system using National Instruments LabVIEW 8.5. LabVIEW was used as the programming language in this application because of its graphical interface that utilizes icons and wires that resemble a flowchart. It allows for the integration of hardware from various manufacturers into the DAQ system and control logic. The sampling rate of the DAQ system was set to 4 Hz. Engine measurement data included atmospheric temperature and pressure, fuel flow rate, compressor discharge temperature and pressure, turbine inlet temperature (T_4), inter-turbine temperatures (ITT), NO_x, premixer shell temperatures, and torque ($\mathcal{T}$). Other engine conditions including shaft power were calculated in real-time using these measurements. Shaft power, given in units of shaft horsepower, was calculated as,

$$\mathcal{P}\ (shp) = \frac{\mathcal{T} \times N_p}{5252} \qquad \textbf{Equation 4.1}$$

where N_p is output shaft speed, held constant at 2000 rpm by the load applied from the water brake dynamometer. Torque was measured in units of $ft \cdot lb$.

4.2 Control Logic

The present fuel controller was developed from an existing DAQ system used for Jet-A and early hydrogen engine testing. The controller that evolved from this system uses DAQ measurements as feedback signals and as triggers for processes that require automatic response. By coupling the fuel control and DAQ systems, fuel pressure and the power output of the engine could be controlled while monitoring their performance. The front panel display produced by LabVIEW VI for the system is shown in shown in Figure 4.1. Fuel controls are consolidated to the top half of the VI front panel and the DAQ measurements are located on the bottom half. A real-time chart of T_4 probe temperatures and premixer shell temperatures provided a visual representation of the measurements.

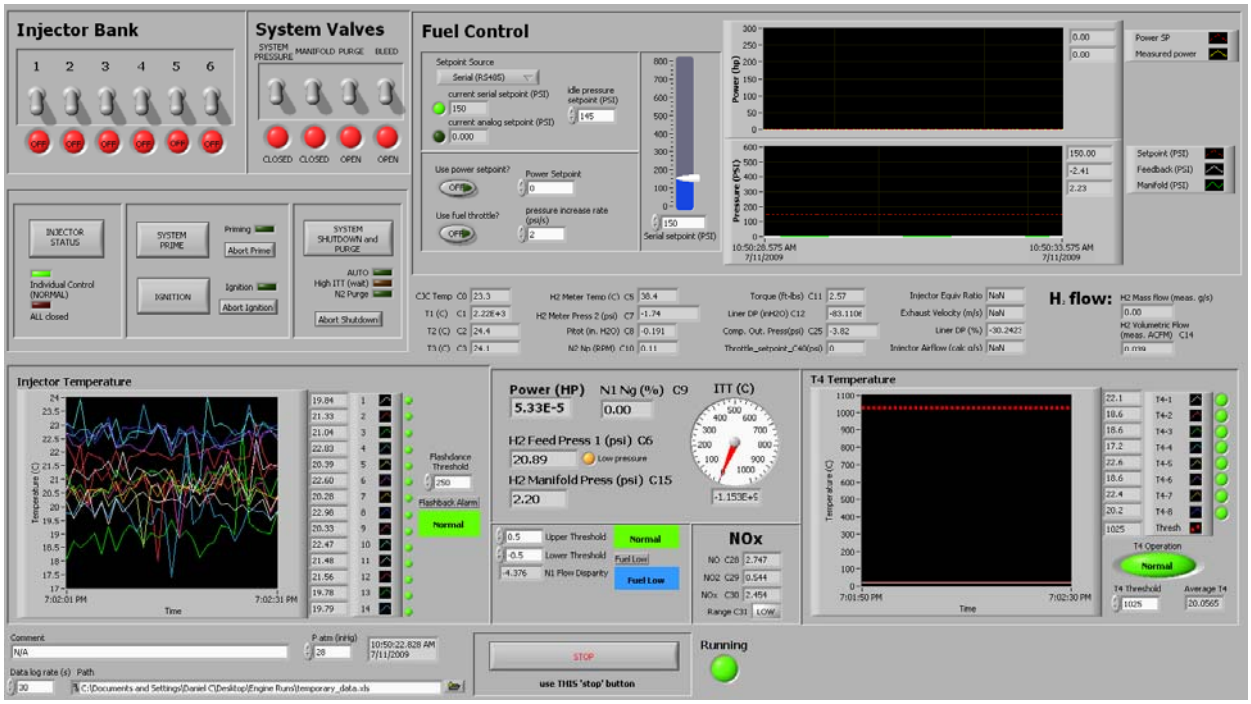

Figure 4.1. Coupled DAQ and fuel control display

The design features automatic procedures for events that have the potential to damage the engine: premixer flashback and high ITT measurements. These control responses are considered engine protection responses. Startup and shutdown procedures were also automated to facilitate engine operation. The following sections describe the two control methods and programming logic of each of the controller functions in greater detail.

4.2.1 Control Methods

Pressure Setpoint

Fuel flow to the engine was controlled by regulating the fuel pressure supplied to the engine from the ER3100 fuel control valve. The control algorithm of the control for the ER3100 is shown in Figure 4.2 [21]. The feedback signal was a 4 to 20mA output signal from a Swagelok pressure transducer rated to 3000 psig.

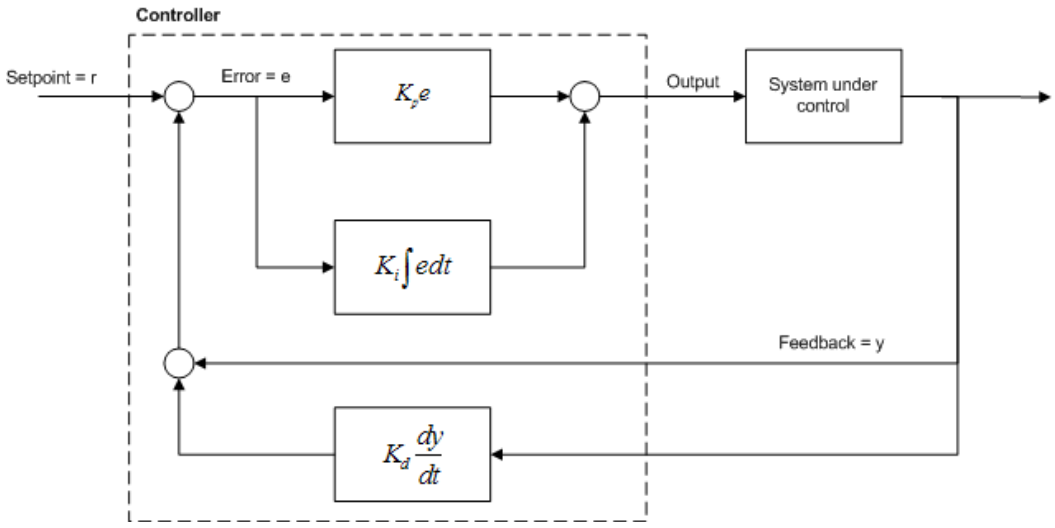

Figure 4.2. Control algorithm for ER3100 [21]

Pressure could be set digitally by using the RS485 computer interface that was integrated with the LabVIEW VI. A pressure setpoint could also be achieved using a power lever that was mechanically linked to a linear potentiometer, shown in Figure 4.3a and Figure 4.3b. From the LabVIEW front panel, the engine operator could toggle between the RS485 (serial) interface and the power lever (analog) to set the fuel pressure. The voltage required for the analog setpoint was provided by a 5 V_{DC} output supply voltage from the ER3100. A wiring diagram for the ER3100 is shown in the appendix.

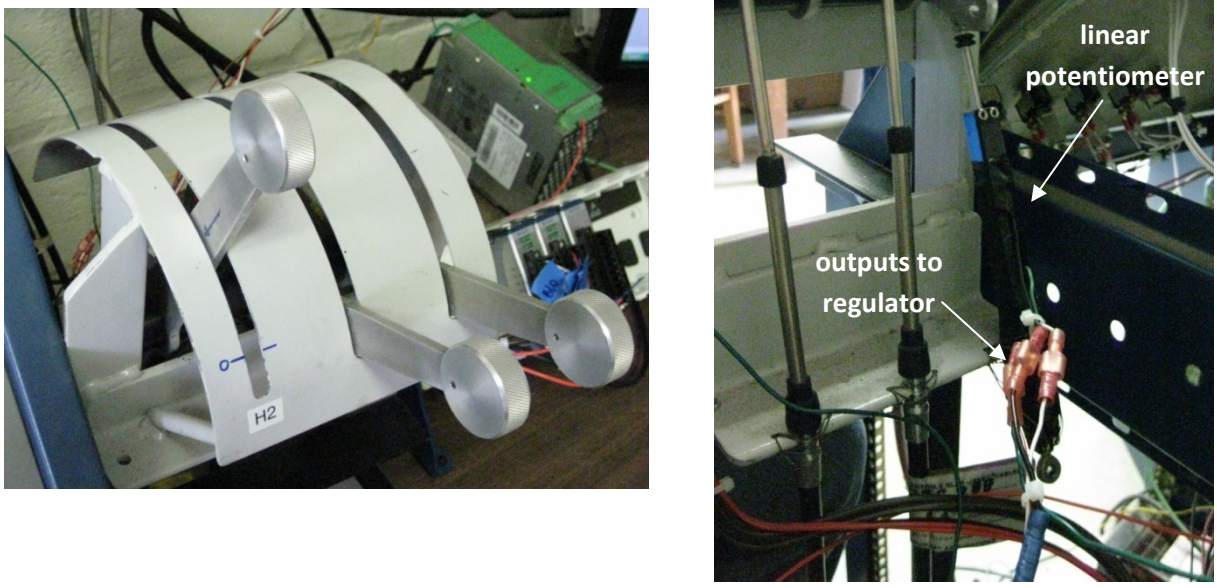

(a) (b)

Figure 4.3. (a) Power lever used for analog control of pressure setpoint, (b) linear potentiometer connection to power lever and pressure regulator

The potentiometer linearly varied the supply voltage from the ER3100 over a 1-5V_{DC} range, corresponding to the 0-3000 psig range of the feedback signal of the pressure transducer. The pressure regulator had a dead zone at voltages less than 1 V_{DC}. To accommodate this characteristic, and to limit the engine fuel supply pressure to 750 psig, the potentiometer output range was limited to 1-2 V_{DC} with a mechanical stop and a resistor voltage divider circuit. The linear relationship between fuel pressure and voltage is given as,

$$Setpoint\ (psig) = 750 \times V_{DC} - 750 \qquad \textbf{Equation 4.2}$$

where 750 is the maximum pressure (psig) that could be seen by the engine at full power, and V_{DC} is the voltage from the electronic regulator that was varied by the linear potentiometer.

Power Setpoint

The shaft power setting was varied by requesting power through the front panel of LabVIEW or through the use of the power lever linked to the linear potentiometer. The operator could choose between the control methods by toggling a switch located on the front panel. Engine shaft power

was maintained using cascaded control loops in which the closed-loop electronic pressure control and the PID-controlled dynamometer loops were inside a feedback power control loop that regulated a desired power setting, as shown in Figure 4.4. The feedback measurement of shaft power was calculated in real-time using Equation 4.1. On the front panel, power could be set by typing in a desired power level or by increasing the requested power level in one horsepower increments.

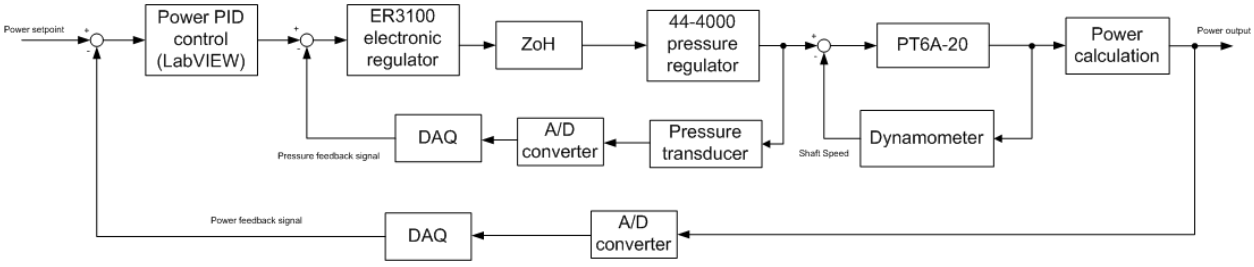

Figure 4.4. Cascaded control loops

When requesting a power level from the engine using the power lever, the analog voltage signal used for setting the fuel pressure was utilized as a dynamic numerical value for calculating a power setting. The linear potentiometer used the 5 V_{DC} voltage source supplied from the electronic regulator as the means for setting this power level, as previously discussed. When using the power lever to request power, the relationship between power and voltage was

$$Setpoint\ (shp) = \begin{cases} 0 & V_{DC} < 1 \\ 550(1 - V_{DC}) & 1 \leq V_{DC} \leq 2 \end{cases} \quad \textbf{Equation 4.3}$$

where V_{DC} was input as the dynamic value read by the DAQ.

In order to activate the power setpoint control, the engine must first be at idle. This was to prevent inadvertent power requests below idle while the engine was still warming up, or power requests different from the current power measurement that could potentially create a step change in fuel flow. The sequence of events needed for toggling to power setpoint control is shown in Figure 4.5. The engine first goes through an automatic priming and ignition sequence, bringing the engine to idle, approximately 58% N_g. The power setpoint control could be

activated after the engine reached steady state at idle, letting the operator request power through the LabVIEW front panel or by throttling the control lever.

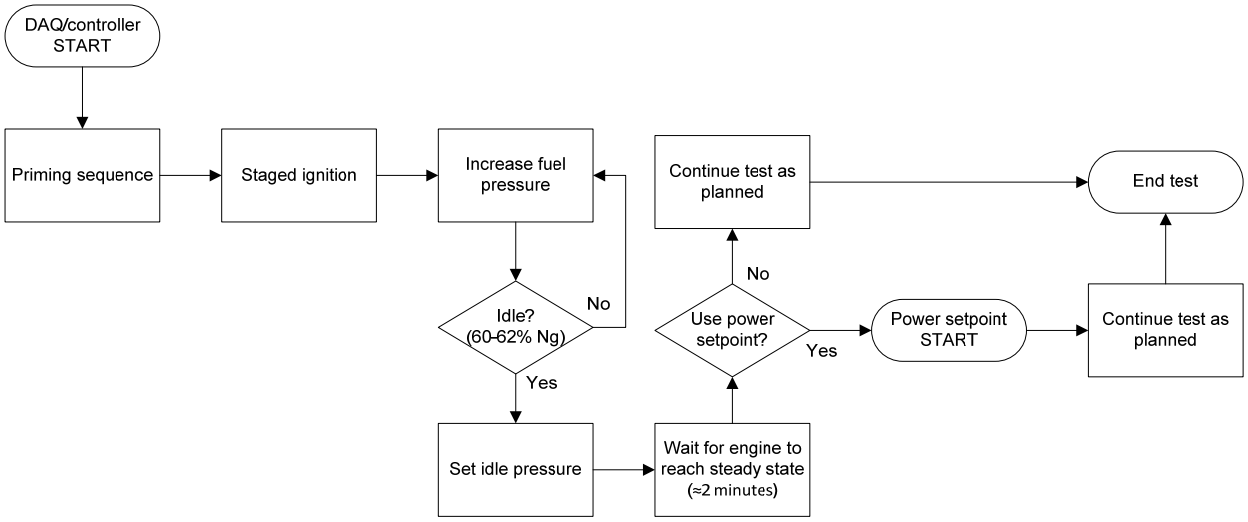

Figure 4.5. Flowchart of actions required to activate the power setpoint controller

Supervisory control of the fuel schedule was incorporated into the control logic since the actual fuel control map of the engine was unknown. An experimental approach to determining a simple control map for this engine is discussed in *Chapter 6*. The rate of change at which the fuel pressure was supplied to the engine, $\frac{dP_{fuel}}{dt}$ (psig/s), was varied depending on the current power level and desired power setting. A flowchart of the power setpoint programming logic is shown in Figure 4.6. It is the same for both front panel and power lever control methods. In the current configuration, when the power measurement is below 200 shp, the allowable $\frac{dP_{fuel}}{dt}$ decreases by 25% when the measured power output is within 10% of the desired setting, therefore decreasing the amount of overshoot. Above 200 shp, the allowed fuel pressure rate of change decreases by 50% when the measured power output is within 5% of the desired power setting. Decreasing the fuel pressure rate of change helped reduce the power overshoot as well as dampen oscillations in power measurements. The required change in the fuel flow derivative above 200 shaft horsepower is due to the increase in engine's turbomachinery efficiency and corresponding increase in sensitivity to changes in fuel flow. Because of the nonlinear characteristics of the engine, it is likely that the PT6A-20 system should see more changes in $\frac{dP_{fuel}}{dt}$ during transient operation than was provided in the present fuel schedule. From the literature, the power level is

considered to be at steady-state when the error between the response and request is less than 2% [22].

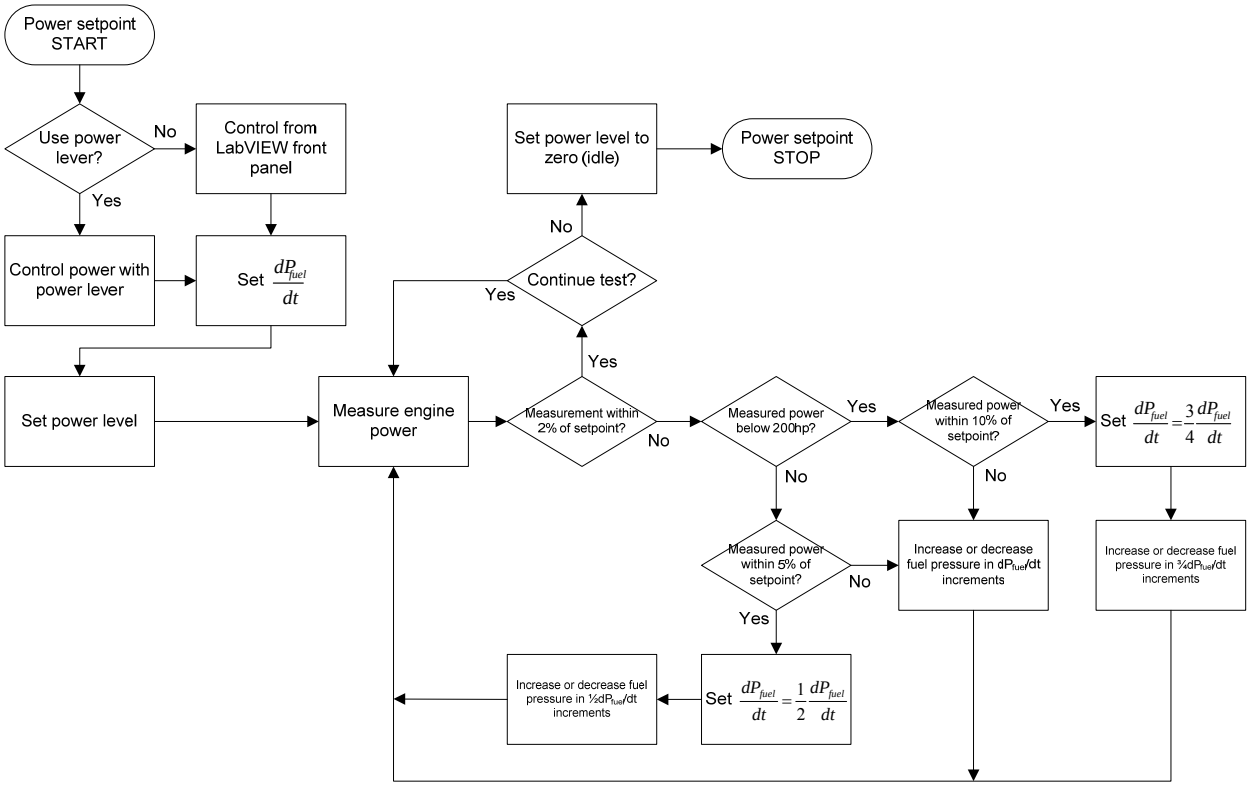

Figure 4.6. Flowchart of power setpoint programming logic

4.2.2 Operability

Flashback logic

The DAQ system displayed a real-time chart of temperature readings from the thermocouples located on the premixers. Throughout every experiment the premixers were constantly checked by the controller for high temperatures that correspond to a flashback. A flowchart of the flashback programming logic for a given engine test is shown in Figure 4.7. If a flashback occurred before the idle conditions were met, all injector banks were closed and fuel flow was reduced to zero. For flashbacks above idle conditions, the fuel controller automatically closed the pneumatic valve of the bank associated with the suspect premixer to prevent damage to the engine. At the same moment that the bank closed, the fuel pressure reduced to one corresponding to a predetermined idle condition. When the premixer temperature decreased to

below the flashback temperature threshold, its matching bank was re-opened to avoid rich combustion in the remaining premixers. Engine tests resumed once all premixer thermocouples measured similar temperatures.

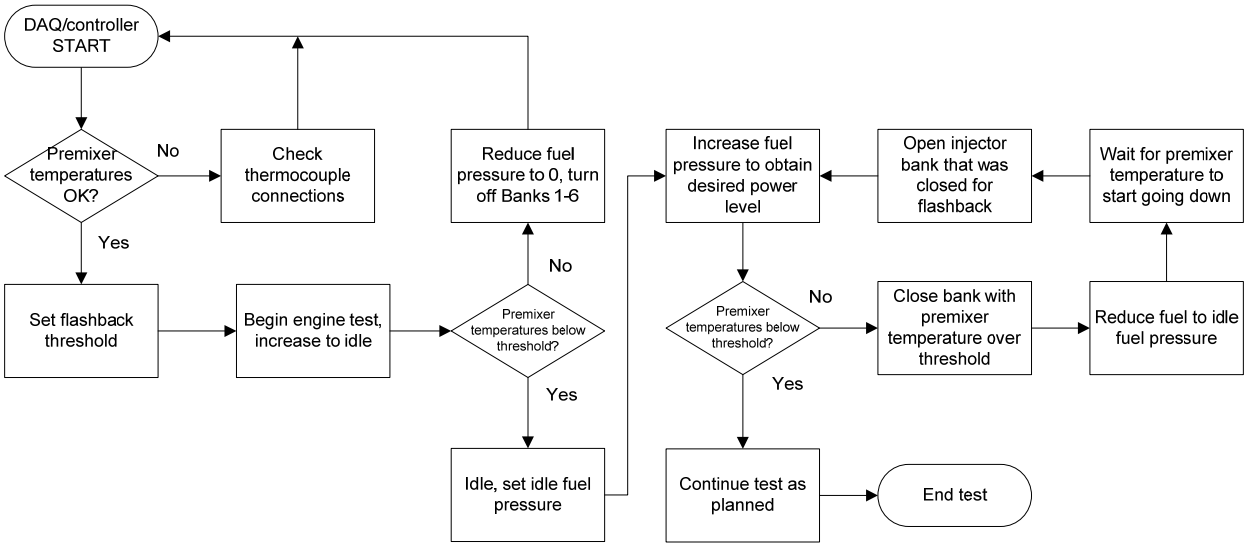

Figure 4.7. Flowchart of programming logic for flashback procedures

High Inter-Turbine Temperature logic

ITT measurements were also monitored by the DAQ system during engine operation. As the engine accelerates, N_g increases, providing more air and cooling to the engine. Because there is a lag in N_g as fuel flow increases, ITT reaches temperatures during engine acceleration that are higher than those at idle or steady operation. High ITT temperatures within limits do not warrant a return to idle, but they do require a reduction in fuel pressure and $\frac{dP_{fuel}}{dt}$ for hydrogen testing.

The flowchart for the high ITT programming logic is shown in Figure 4.8. When ITT reaches a temperature higher than 750 ^{o}C but lower than 800 ^{o}C the power setting is allowed to continue to be controlled by the operator for 15 seconds. After this time, the controller takes over and begins to reduce the fuel pressure until ITT reaches a temperature under the limits. When ITT has gone below the limits, power control is returned to the operator. Should the ITT measurements show a reading above 800 ^{o}C, the controller begins reducing fuel pressure after five seconds until ITT is below the temperature limit. Finally, if ITT measurements are higher than 1000 ^{o}C, the controller takes over and immediately reduces the fuel pressure to a level corresponding to idle to prevent damage to the hot section. The power setpoint is set to zero and the power setpoint

toggle switches are deactivated. Temperature limits and time spent above each limit can be changed from the defaults by the operator at any point during engine operation.

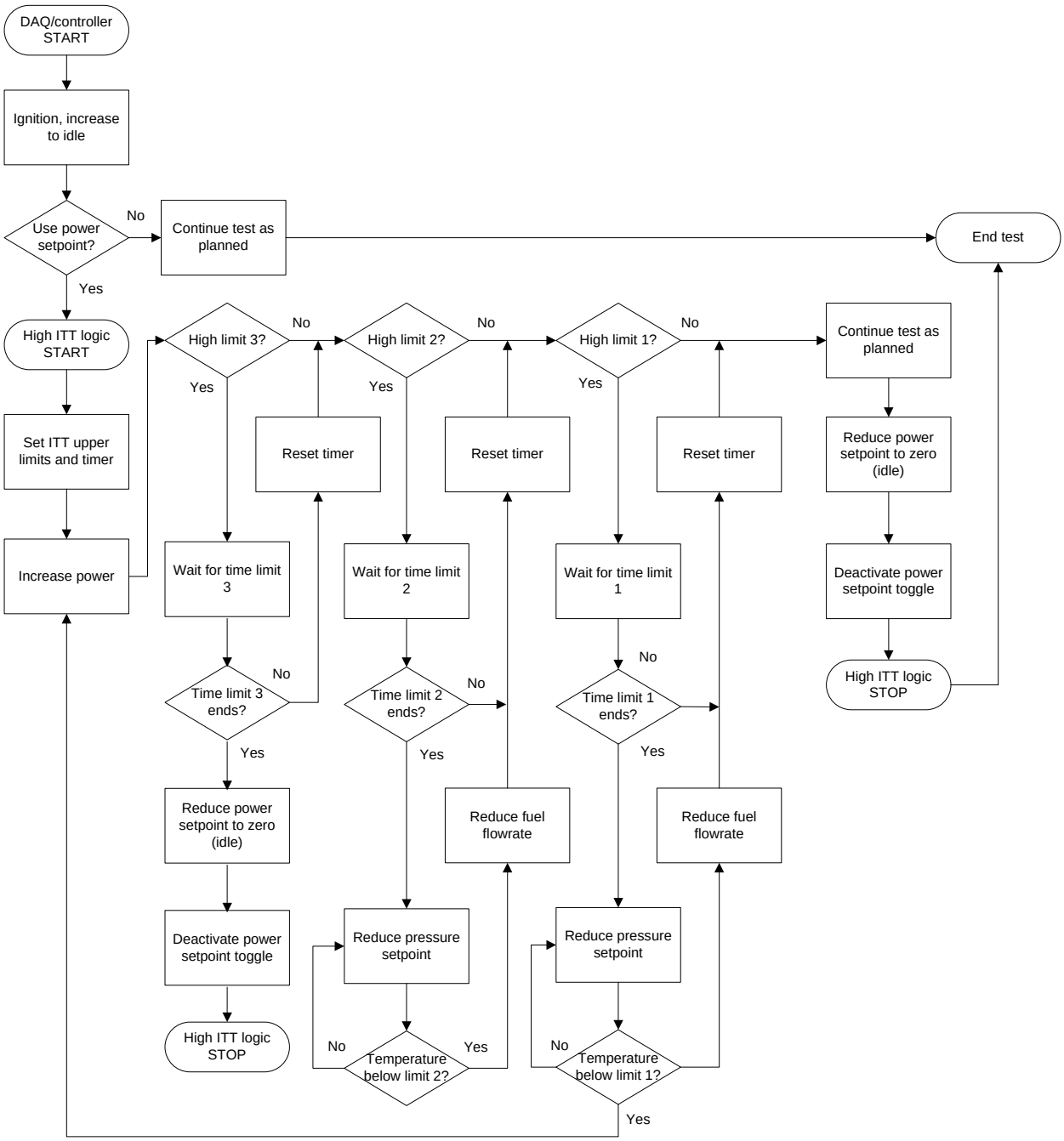

Figure 4.8. Flowchart of programming logic for high ITT when using power setpoint. Defaults for ITT limits are (3) 1000 ^{o}C for 0.5s, (2) 800 ^{o}C for 5s, and (1) 750 ^{o}C for 15s.

The allowed limits for ITT were based on previous temperatures seen during hydrogen engine testing and the normal engine operating limits given in the PT6A-20 Training Manual [23]. A more detailed table of operating limits for the PT6A-20 on Jet-A fuel is given in the appendix. The ITT logic activates when the engine is controlled using power setpoints. It was assumed the operator would reduce the fuel pressure when operating the engine using only the electronic pressure regulator.

4.2.3 Automated Operations: Priming, Ignition, and Shutdown

Another part of the programming logic is the sequence of events related to the preparation of the engine for ignition (engine priming), engine ignition, and the shutdown and nitrogen purge of the fuel system. The actions associated with each of these events were automated for minimal operator input in order to prevent valves from opening and closing in the incorrect order or at an inappropriate time. An abort trigger was available in case the automatic operations needed to be stopped.

Priming Sequence

Engine priming allowed hydrogen to enter the entire fuel supply system, setting the fuel pressure in the fuel manifold upstream of the combustion chamber to a predetermined level. After priming, the engine was ready for ignition. With the engine starter and igniters on, the premixer banks were opened in succession to bring the engine to idle.

A flowchart for engine priming is shown in Figure 4.9. To prime the engine for ignition, the purge and bleed valves were closed and the system pressure and manifold valves were open, letting hydrogen flow to the electronically-controlled pressure regulator. The operator then turned on the engine starter and the premixer banks were all opened while the pressure setpoint was increased to 150 psig. This started hydrogen flow through the engine as it was being motored by the starter. All the banks were simultaneously closed after the hydrogen had been flowing through the engine for ten seconds.

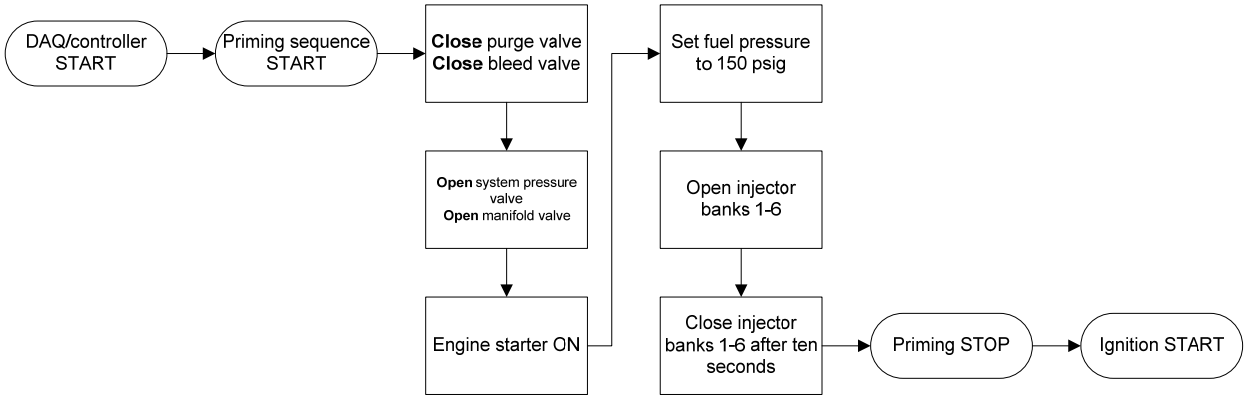

Figure 4.9. Flowchart of automatic engine priming sequence

Ignition

After the priming sequence, the automatic ignition sequence could be initiated. The T_4 probes that were installed in the engine provided measurements of the combustion temperatures. Figure 4.10 is a flowchart of the procedure for automatic ignition. With the igniters and starter on, Bank 2 was opened to begin hydrogen flow into the engine. Combustion was indicated by a rise in T_4. If combustion did not occur within ten seconds, the premixer bank was closed and the igniters and engine starter were turned off. The procedure was then repeated with a higher manifold pressure. If the DAQ indicated a rise in T_4, premixer banks 1, 4, 6, and 3 were opened sequentially in 0.5 s increments to bring the engine to 55%, just below idle. Bank 5 was opened when T_4 and ITT had stabilized, idling the engine at 58% N_g. The order in which the banks were opened was based on early engine testing with the premixers to ensure the premixers were adjacent to an ignition source. Idle rotor speed was reached at the end of the ignition sequence, and the test proceeded when engine temperatures and pressures had reached steady-state.

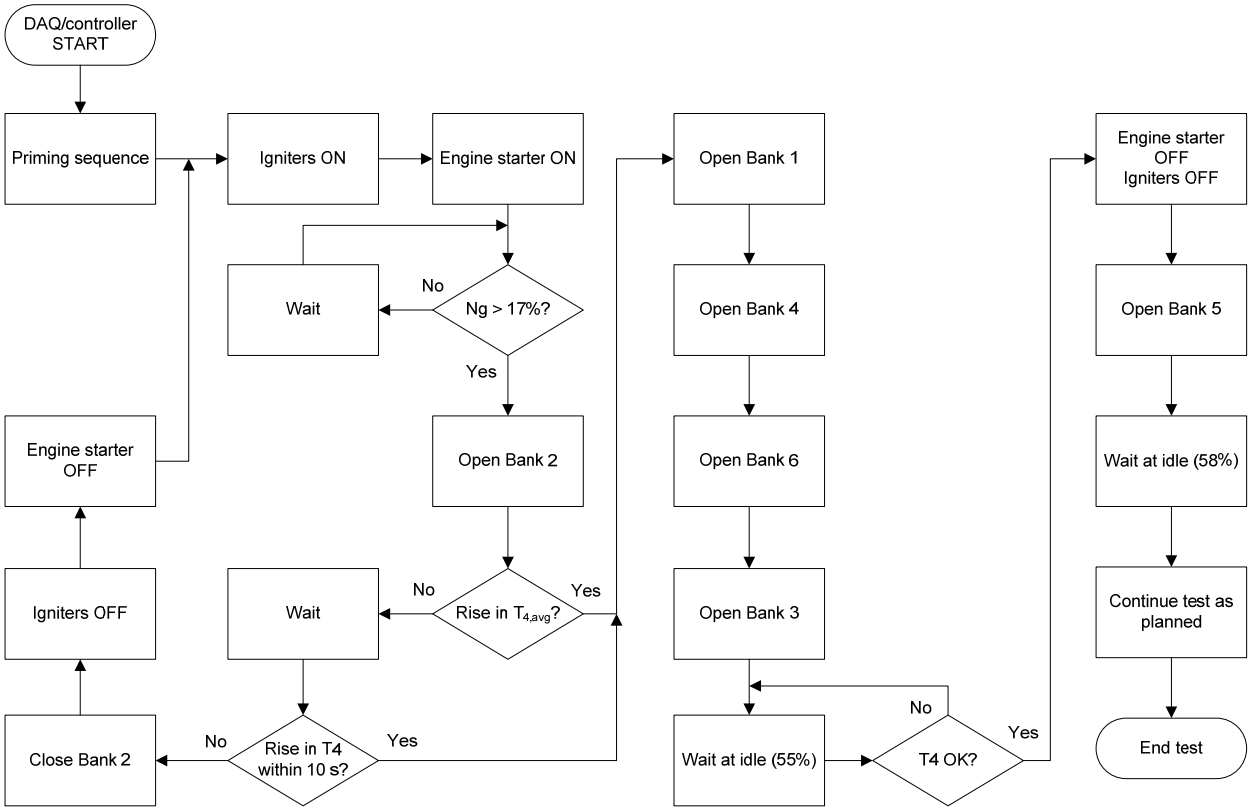

Figure 4.10. Flowchart of automatic engine ignition procedure

Shutdown Sequence

The automatic shutdown procedure, shown in Figure 4.11, was performed when the engine was at idle and at the completion of testing. When the engine was ready for shut down, the premixer banks were all simultaneously closed and the system pressure and manifold valves were closed. The bleed valve was opened to exhaust the remaining hydrogen into the atmosphere and the purge valve was opened to begin flow of nitrogen through the fuel supply lines. After a short period, the purge valve was closed and nitrogen ceased to flow through the fuel lines upstream of the engine. Once the ITT reading had reached a relatively low temperature (to avoid cool nitrogen quenching), the engine starter was turned on and the bleed valve was closed while the purge valve, manifold valve, and premixer bank valves were open. This sequence allowed nitrogen to purge any remaining hydrogen through both the engine and the remaining fuel supply lines. The engine starter was then turned off and the manifold valve, premixer bank valves, and purge valve were closed while the bleed valve remained open, returning the engine to a safe, non-operational mode.

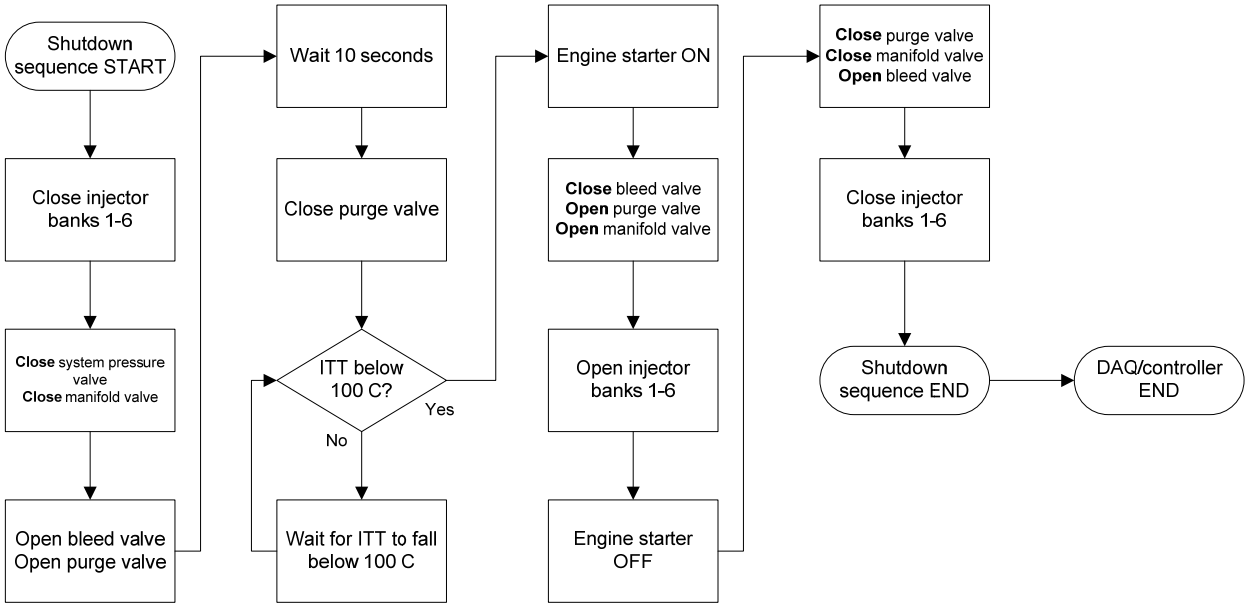

Figure 4.11. Flowchart of automatic engine shutdown procedure

4.3 Summary of DAQ and Control Logic

The fuel control presented acts as both a data acquisition and fuel control system. The controller was designed to protect both the operator and the engine while providing the flexibility of modifying operability limits during tests. The baseline operability of the PT6A-20 on lean premixed hydrogen is dependent on measurements acquired by the DAQ remaining within specified control limits. Additional functions of the controller included pressure and power setpoint control methods, automatic operations, and visual representations of temperatures being measured. The next chapter discusses the performance of several of these control functions during engine operation.

Chapter 5: Controller Results and Discussion

This section describes in detail the tuning procedure for the electronically controlled pressure regulator and analyzes the performance of different fuel control functions during routine engine testing. The tuning procedure applied is first introduced, followed by the performance of the regulator under both serial and analog pressure control methods. Finally, engine response for different control methods and functions of the fuel controller are shown and discussed.

5.1 Electronic Regulator Tuning

With the electronic pressure regulator installed in the fuel supply line, the next step was to tune its controller. Initial analysis of the dynamics of the pressure regulator proved to be too complicated to attempt an analytical approach to tuning the gains of the controller, therefore the gains were determined experimentally. The software provided by Tescom for the ER3100 electronic regulator was integrated with the LabVIEW control VI and the final control gains were chosen after running a series of nitrogen (N_2) and helium (He) tests. The pressure transducer located downstream of the electronic regulator provided the feedback signal for the closed loop control system, shown in Figure 5.1.

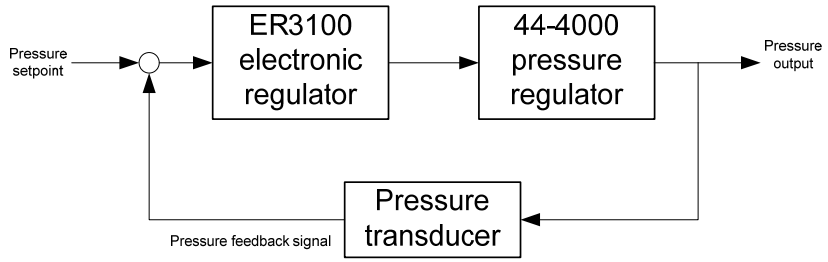

Figure 5.1 Pressure control system consisting of ER3100 controller, pressure regulator, and pressure tranducer

To begin the tuning process, a Ziegler-Nichols method was applied in order to experimentally determine the PID gains, as suggested by Ogata in *System Dynamics* [22]. The general equation for a PID controller in the Laplace domain is given as

$$G_c(s) = K_p\left(1 + \frac{1}{T_i s} + T_d s\right) \qquad \textbf{Equation 5.1}$$

where K_p is the proportional gain, T_i is the integral time, and T_d is the derivative time. Equation 5.1 can also be written as

$$G_c(s) = K_p + \frac{K_i}{s} + K_d s \qquad \textbf{Equation 5.2}$$

where $K_i = \frac{K_p}{T_i}$ is the integral gain and $K_d = K_p T_d$ is the derivative gain. With a system tuned using the Ziegler-Nichols method, a unit-step input results in an S-shape response curve that has, on average, approximately 25% overshoot. The procedure begins by setting $K_i = K_d = 0$ and the gain K_p is increased from zero until the response shows sustained oscillations with the amplitudes of each peak approximately equal. These oscillations correspond to a critical proportional gain value, K_{cr}. The PID gains are then based off K_{cr} and the period of the oscillations, P_{cr}. A table of the tuning rules using K_{cr} and P_{cr} for different controller types is shown in Table 5.1. The tuning rules apply directly to Equation 5.1. This technique, however, did not succeed for the ER3100 since the step input applied resulted in the controller-regulator system becoming almost immediately unstable without values for K_i and K_d.

Table 5.1 Ziegler-Nichols tuning rule based on critical gain K_{cr} and critical period P_{cr} [22].

Type of Controller	K_p	T_i	T_d
P	$0.5K_{cr}$	∞	0
PI	$0.45K_{cr}$	$\frac{1}{1.2}P_{cr}$	0
PID	$0.6K_{cr}$	$0.5P_{cr}$	$0.125P_{cr}$

In the second tuning attempt, the Ziegler-Nichols method was combined with the tuning procedure suggested by the Tescom ER3100 literature [21]. The beginning of the Tescom procedure was similar to that of the Ziegler-Nichols technique with $K_i = K_d = 0$, but the initial K_p gain was fixed at $K_p = 200$ which was a higher starting value than expected. Sustained oscillations began at $K_p = K_{cr} = 400$ resulting in a $P_{cr} \approx 4s$. From Table 5.1 for a PID controller, this produces $K_p = 240$, $T_i = 2$, and $T_d = 0.5$. Combining this with the constants from Equation 5.2 gives $K_p = 240$ and $K_i = K_d = 120$.

Using these preliminary gains, the controller was further tuned to provide a faster response, better steady-state response, and less overshoot and pressure oscillations. From the Tescom control loop shown in Figure 4.2, the derivative gain is the rate of change of the feedback signal and not the derivative of the error signal. This is indicative of the control loop containing feedback resembling a pseudo-derivative feedback (PDF) control described by Phelan in 1977 [24]. Pseudo derivative feedback is similar to a PID compensator, but does not produce the associated system zeroes and has a higher emphasis on critically damped and overdamped systems. An advantage to PDF is that the derivative gain can be increased to near infinity, with the consequence being that the system response to a reference input will converge to that of a normal proportional control system [24]. The algorithm also eliminates the derivative error spikes associated with step changes in setpoint. Moreover, PDF control systems are less expensive, easier to implement, and less sensitive to noise [25].

When applied to the ER3100, the gain for K_d was increased to its final value in order to eliminate overshoot and decrease the amplitude of the steady-state oscillations while still

providing a fast response. Additional tuning of K_p and K_i resulted in a system that for a step input of 100 psig had a step response time of less than 3 s, no overshoot and steady-state error less than 2% as shown in Figure 5.2. The feedback offset when the setpoint is zero is due to the pressure transducer not being zeroed before the beginning of the test. Further experiments with a zeroed pressure transducer demonstrated this to not be a problem since the controller performance did not show signs of change. The final PID gains used throughout the remainder of engine tests are given in Table 5.2.

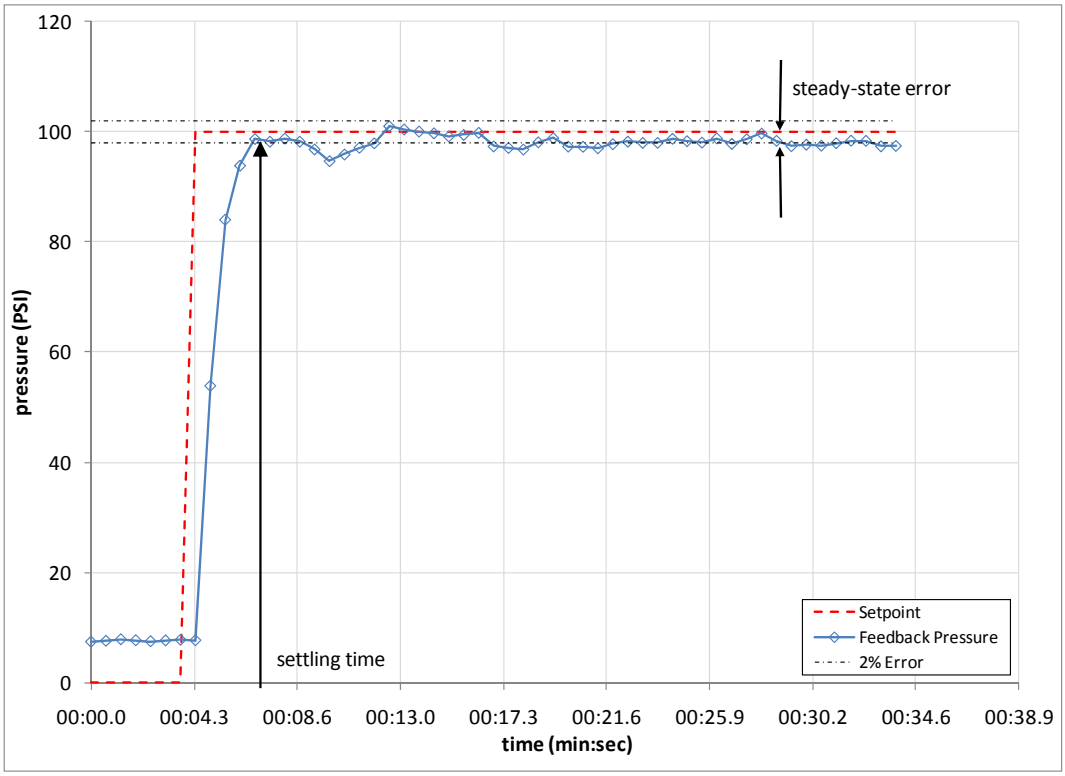

Figure 5.2 Step response for pressure control system

Table 5.2. PID gains for ER3100

K_p	K_i	K_d
275	90	280

5.2 Controller Performance

Helium was used to verify the performance of the controller since helium has a molecular weight only double that of hydrogen. The first series of pressure tests using the final PID gains showed the output response to different step inputs for both serial and analog pressure control methods (recall that serial and analog control was provided for panel input and power lever control, respectively). A plot of the step responses for serial and analog control is shown in Figure 5.3 and Figure 5.4, respectively. A step input of no more than 100 psig was applied during these pressure tests (sudden increases in fuel pressure during engine testing have the potential to surge the engine, therefore the electronic regulator was tuned accordingly). At higher pressures, the steady state error increased to 3%. Increasing the integrator gain K_I would likely reduce the steady-state error at these pressures, but might reduce system stability.

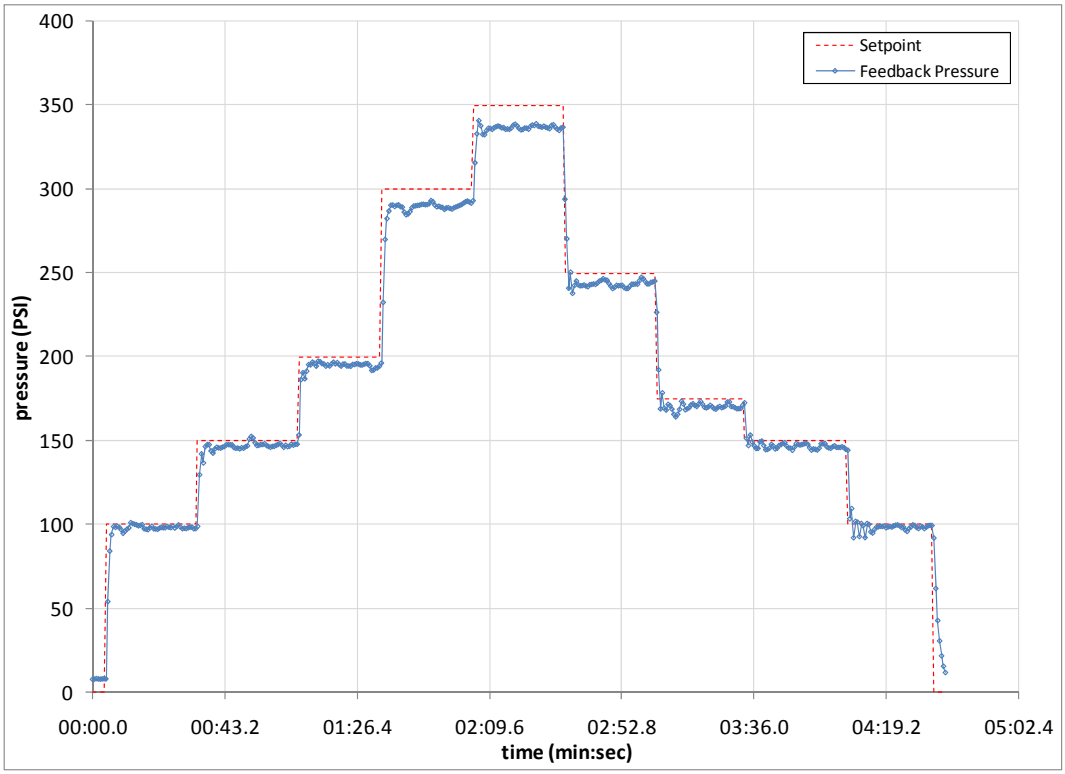

Figure 5.3. Time response plot of the electronic regulator for various pressure step inputs using serial setpoint

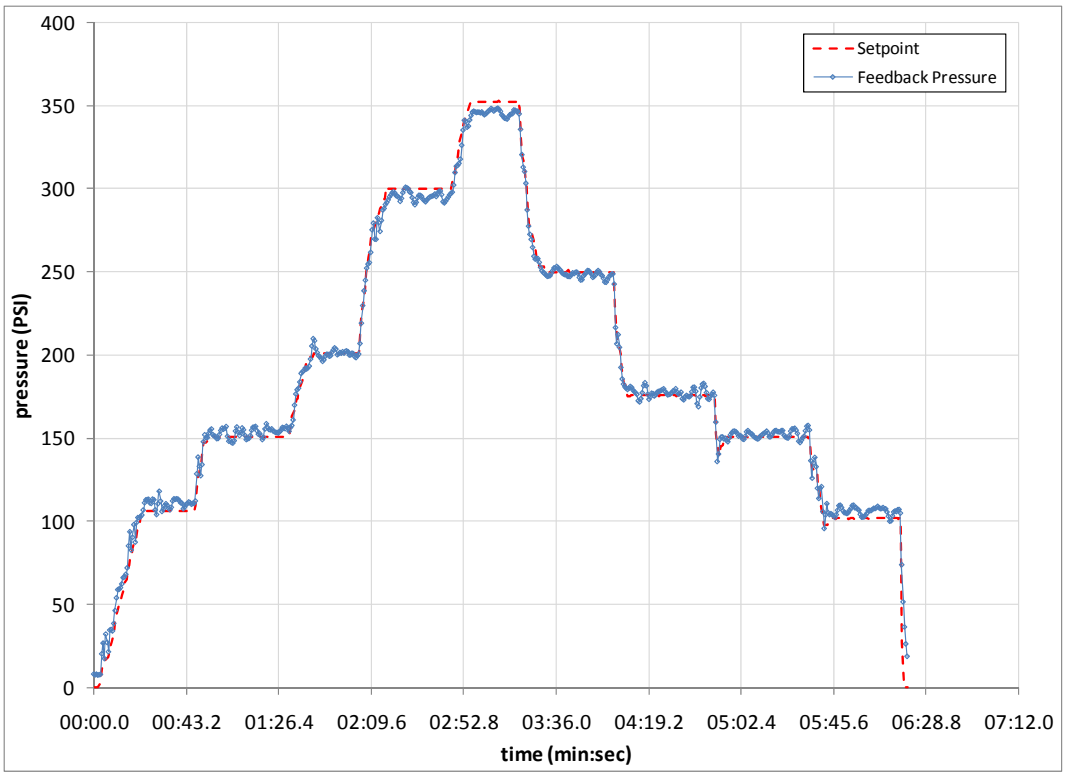

Figure 5.4. Time response plot of the electronic regulator for various pressure inputs using analog setpoint

A flashback was simulated during a second series of pressure tests to determine the response time of the regulator should a step-down in pressure occur during a hydrogen engine test. The simulated flashback using serial control, shown in Figure 5.5, occurs at 200 psig (corresponding to approximately 100 shp). The pressure setpoint drops to the idle pressure with the controller responding in approximately one second, demonstrating the quick flashback response of the fuel controller. A similar test was performed using analog pressure control, with results shown in Figure 5.6. An observation of note is that a step-down in pressure from a high pressure setpoint results in a larger overshoot. To compensate for this, a manual low pressure regulator (LPR) was installed parallel to the electronic regulator and kept at a constant 120 psig during engine runs. The LPR serves two purposes: it provides a manual pressure control should the electronic regulator fail, and eliminates the overshoot seen in pressure testing. A step-down change in pressure with the LP regulator in operation is shown at the end of the test in Figure 5.5.

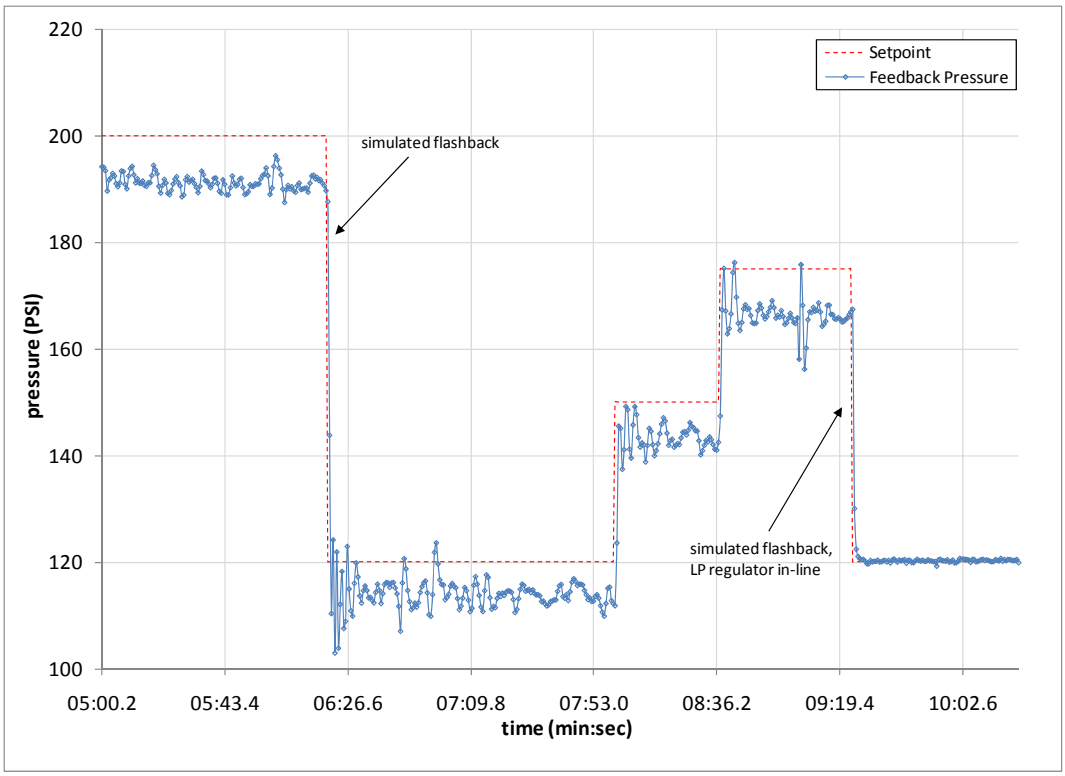

Figure 5.5. Time response plot of ER3100 pressure testing after initial PID gains have been set using serial control mode

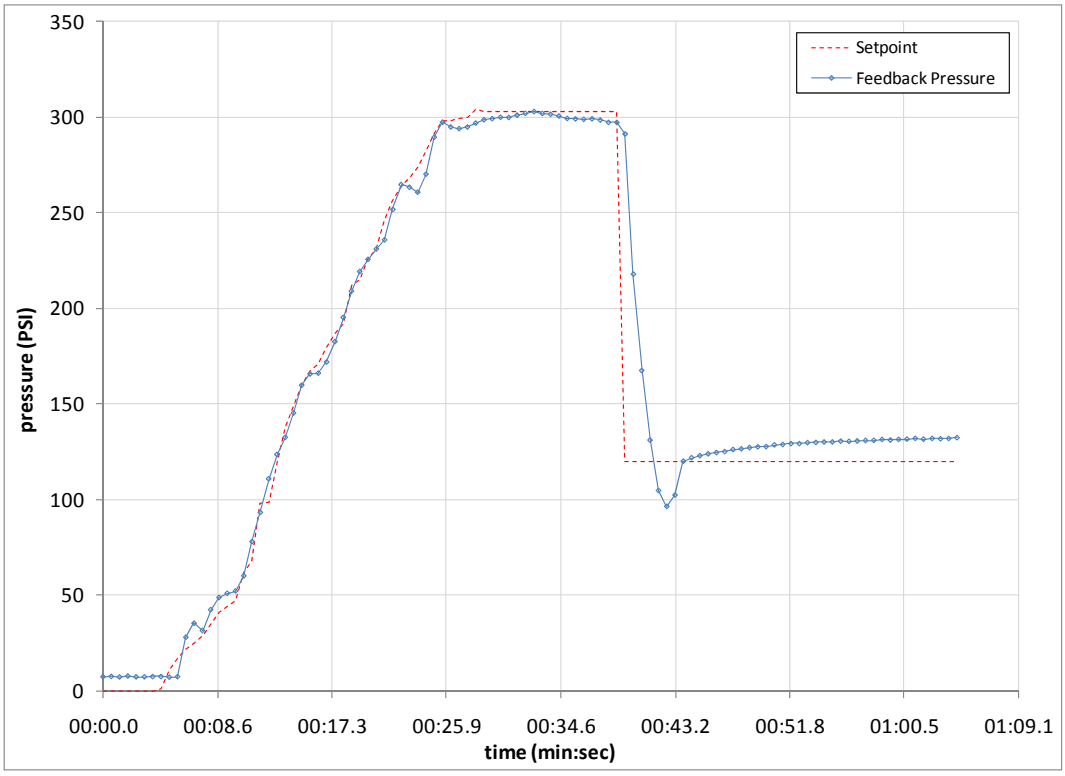

Figure 5.6. Time response plot of ER3100 for analog setpoint flashback simulation

The decaying inlet characteristic of the electronic regulator was also tested as the feed pressure decreased. The feed pressure was nominally 800 psig during an engine test; however, extended engine experiments often ran the fuel supply low and decreased the feed pressure. With the previous fuel control system, an operator managed a pilot regulator to vary the fuel pressure to the engine. As the feed pressure decreased, the regulator had difficulties maintaining a fixed fuel pressure. The operation of the electronic regulator with decreasing feed pressure is shown in Figure 5.7. The plot shows that the regulator did not show changes in output pressure until the feed pressure was approximately equal to that of the setpoint. Engine testing was normally completed before the feed pressure fell below 400 psig.

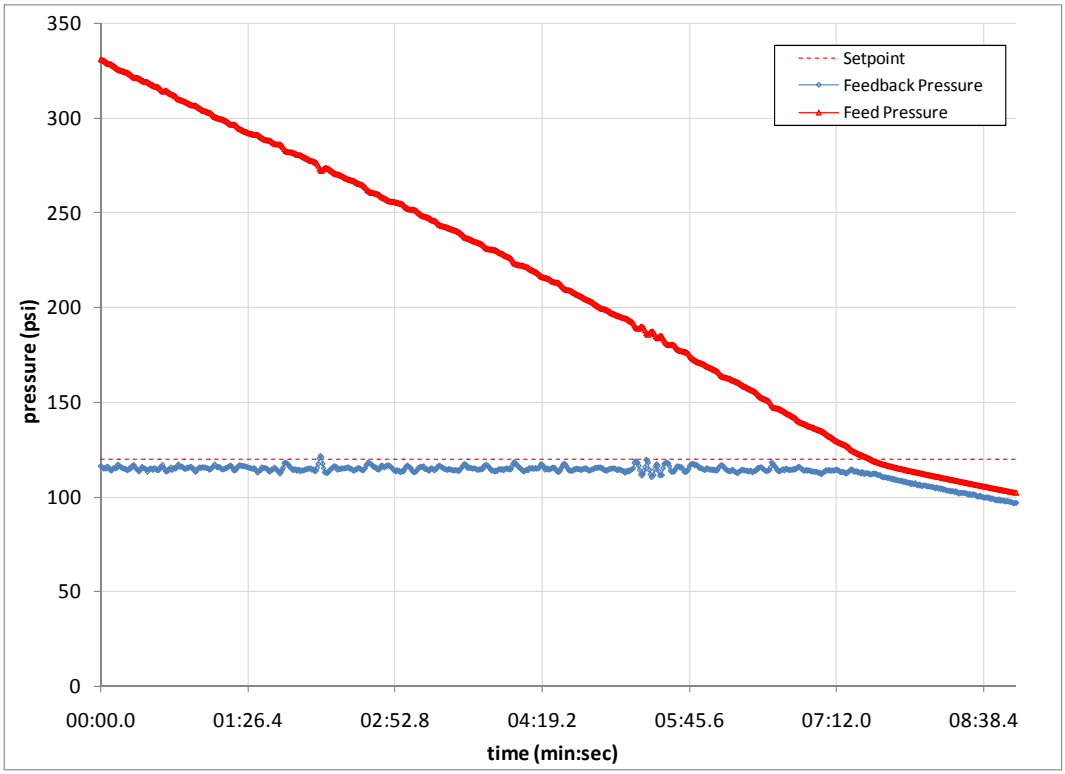

Figure 5.7. Time response plot of ER3100 pressure testing with decreasing feed pressure

5.3 Engine Performance

As different functions of the fuel controller became available they were tested individually in separate engine tests. Operational limits of the engine were largely taken into consideration during controller experiments. For example, flashbacks routinely occurred near the 150 shp level with the 18-premixer combustor design. To protect the engine, the majority of fuel control testing was performed between idle and 100 shp, including simulation of the flashback control logic. Engine operation for each of the functions described in the previous chapter is presented here in two parts, the first describing the performance of the engine with the different control methods, and the second demonstrating the automatic functions. Recommendations for testing the limits of the controller (assuming full range engine operation) are included in Section 7.2.

Control functions not presented in this section had insufficient data to warrant a detailed description or they were not tested. The priming and shutdown sequences (not including the purge sequence) successfully worked during each engine test after being programmed. Data during these processes were not recorded because these procedures were simply the flow of hydrogen or nitrogen through the fuel system at timed intervals. Data collection began when the engine starter was turned on in preparation for ignition. High ITT logic was the only control function not tested in either combustor design. Throughout the series of experiments run on the engine, including controller and redesigned premixer testing, ITT did not cross any of the preset thresholds included in the controller.

5.3.1 Control Methods

Pressure Setpoint

Preliminary tests using the electronic pressure regulator confirmed two design criteria for the operation of the PT6A-20 with hydrogen: fuel mass flow is proportional to fuel pressure, and the pressure regulator was able to adequately maintain a pressure request. The first design criterion is visually verified in Figure 5.8, which shows H_2 mass flow and engine power output as a function of fuel pressure as the pressure setpoint was increased and decreased during the experiment. The grouping of data points correspond to ignition, idle, and 100 shp. Mass flow and pressure increase linearly to 100 shp, though an analysis by Perry suggests that inaccurate measurements by the hydrogen metering equipment is the likely cause for deviations from the linear trend near and above 100 shp [18].

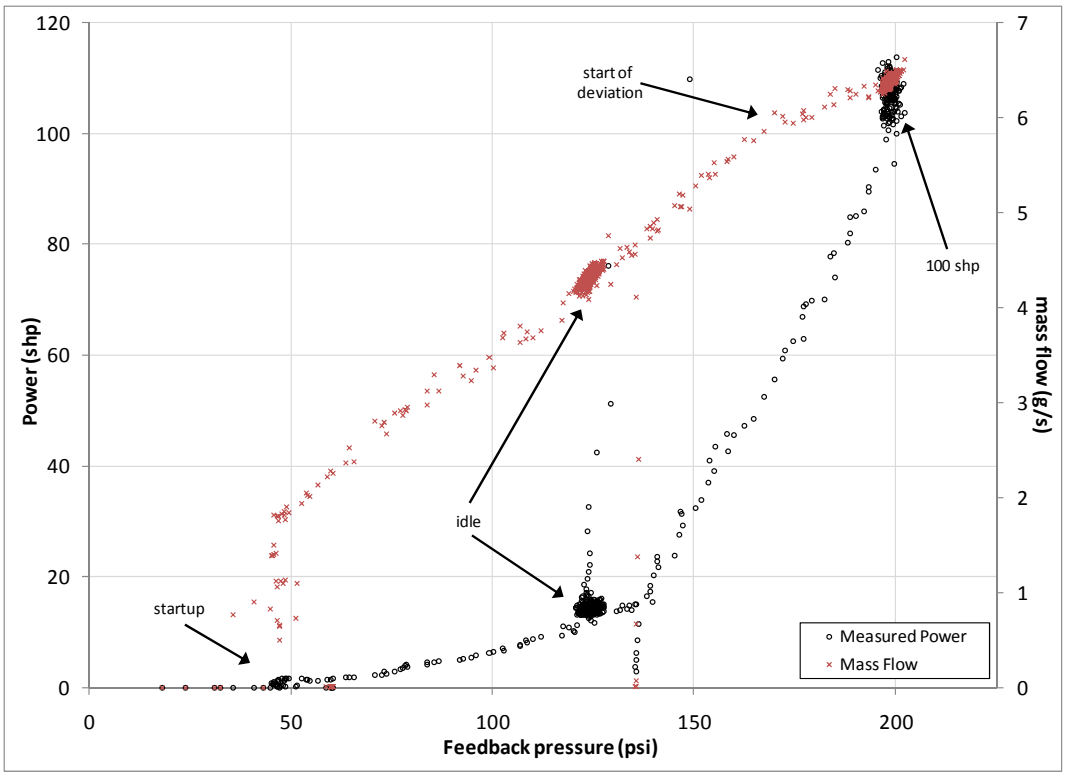

Figure 5.8. Power and H_2 mass flow as a function of feedback pressure with 18-premixer design

At 100 shp the fuel pressure and thus mass flow is kept constant. This is shown more clearly in the time trace of engine power, fuel mass flow, and fuel pressure in Figure 5.9. The second criterion of the controller's ability to maintain a pressure setting is also better seen in Figure 5.9. When the fuel pressure is kept fixed at approximately 200 psig, the engine power trends upward over time at the same fuel pressure since the compressor outlet temperature continues to rise until steady-state.

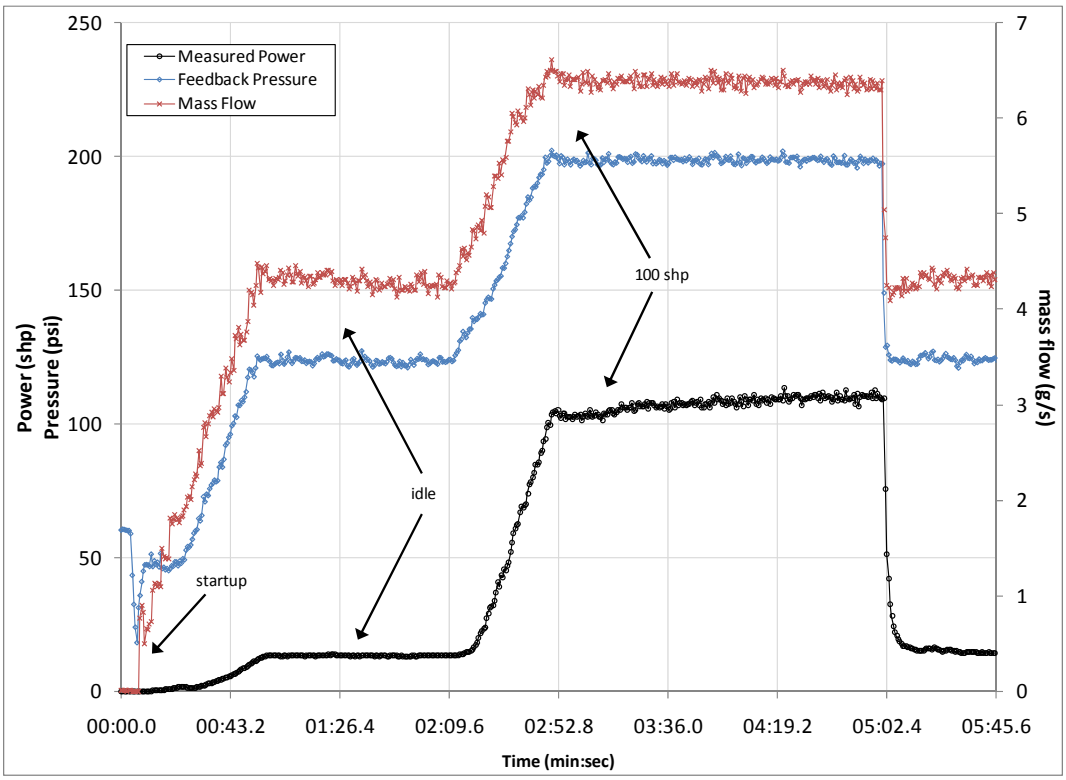

Figure 5.9. Power, pressure, mass flow during engine run to 100 shp with 18-premixer design

Power Setpoint

The initial tests using power level requests used only the VI front panel (serial input), with step inputs for power request. The fuel pressure rate of change was set at $\frac{dP_{fuel}}{dt}$ = 2 psi/s, both on acceleration and deceleration. A plot of the engine performance from this test is shown in Figure 5.10. The pressure setpoint is also displayed to show the compensation of the inner pressure control loop of the system illustrated in Figure 4.4. Power fluctuations in this test were ± 10 shp.

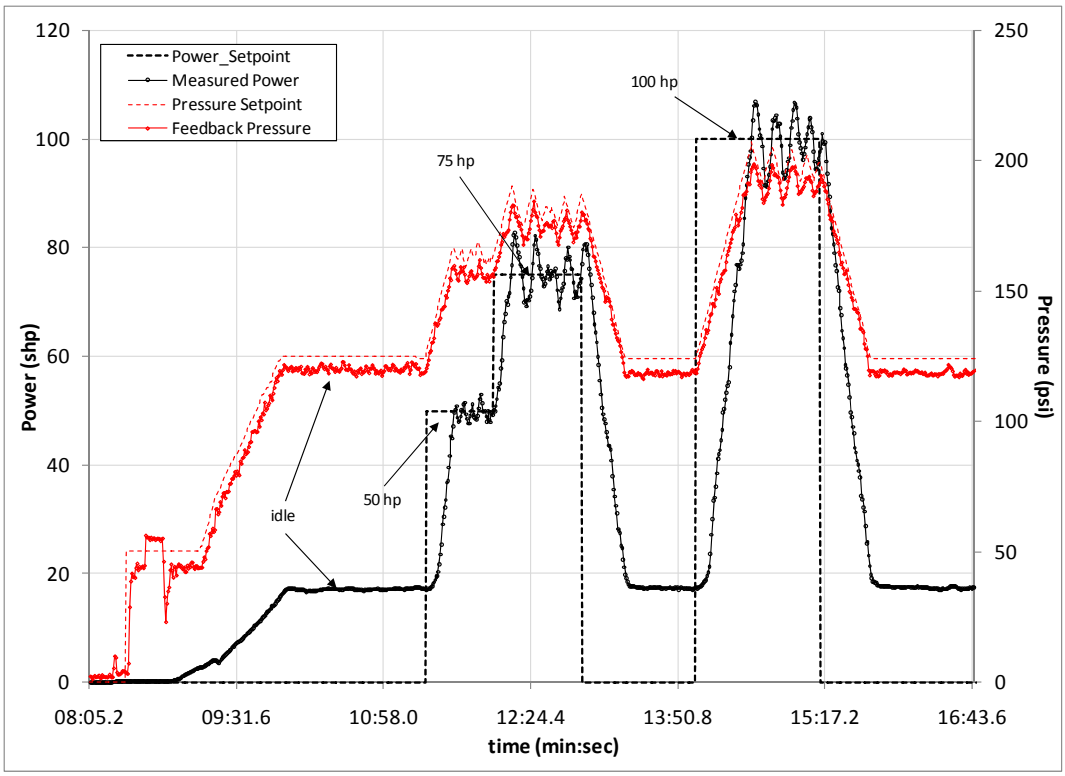

Figure 5.10. Performance at different power level setpoints

The relatively large oscillations in power (up to 10%) led to the addition of the rate control described in Section 4.1. A plot of the resulting controller response to a 100 shp request is shown in Figure 5.11. The rate of fuel pressure change decreases when the measured power comes within 10% of the setpoint, helping reduce the oscillations seen at steady state. Power fluctuations decreased to ±5 shp for this test, a variation that was seen during early engine testing with manual fuel pressure regulation. The periodic oscillations at 100 shp could be from the combination of the gains chosen for the power control as well as from the dynamometer attempting to maintain the shaft speed at 2000 rpm. Also shown in Figure 5.11 is the response of the controller with power request by the use of the power lever. Power output measurements were also approximately ±5 shp.

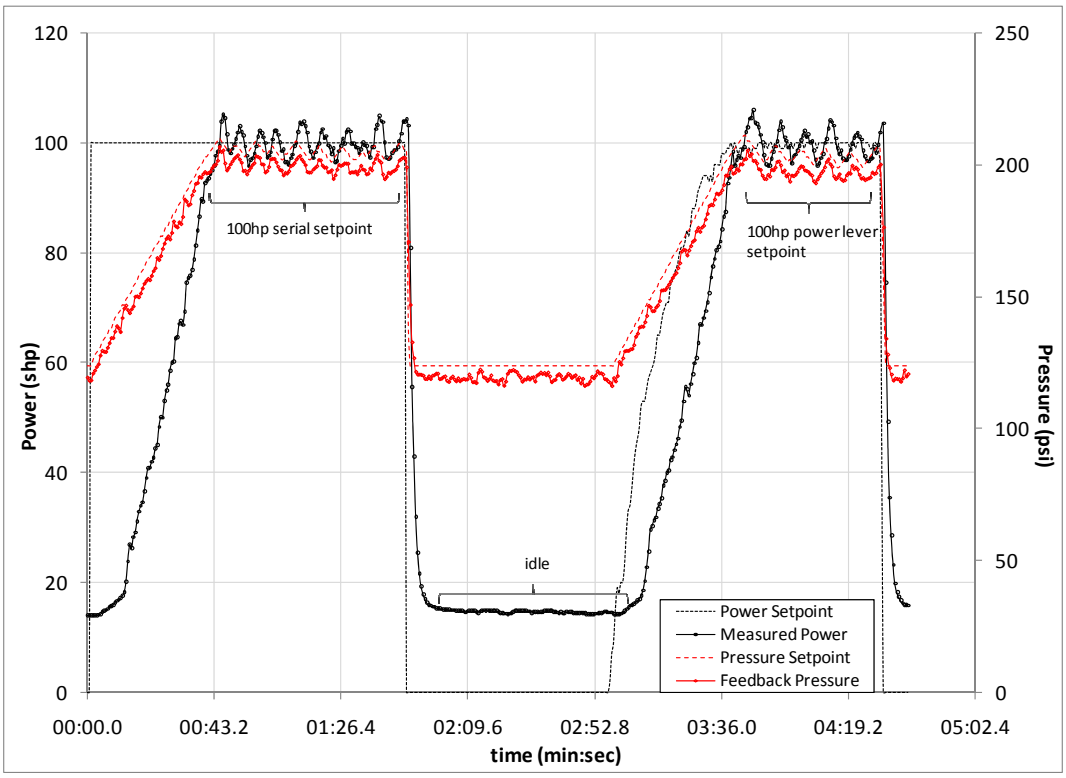

Figure 5.11. Engine response with serial and power lever setpoints with controller rate control in place

5.3.2 Operability

Flashback simulation

Because of the conservative operation of the engine during controller experimentation, the flashback control logic initially was not tested directly, but rather simulated in a controlled manner. The experiment tested the ability of the controller to disengage the analog pressure control (via power lever) method and return to the idle pressure. While the engine was accelerating, a simulated high temperature was input into the control system. The controller registered this as a temperature above the flashback temperature threshold and took the appropriate actions according to its programmed logic.

The response of the engine to this simulation is shown in Figure 5.12. The premixer bank associated with the mock high temperature was closed and the engine returned to idle. The dip in power level after the simulation is from the engine operating at idle without all six premixer banks open. Correct idle conditions were resumed when the premixer bank was reopened, allowing hydrogen to flow again through all fourteen or eighteen premixers.

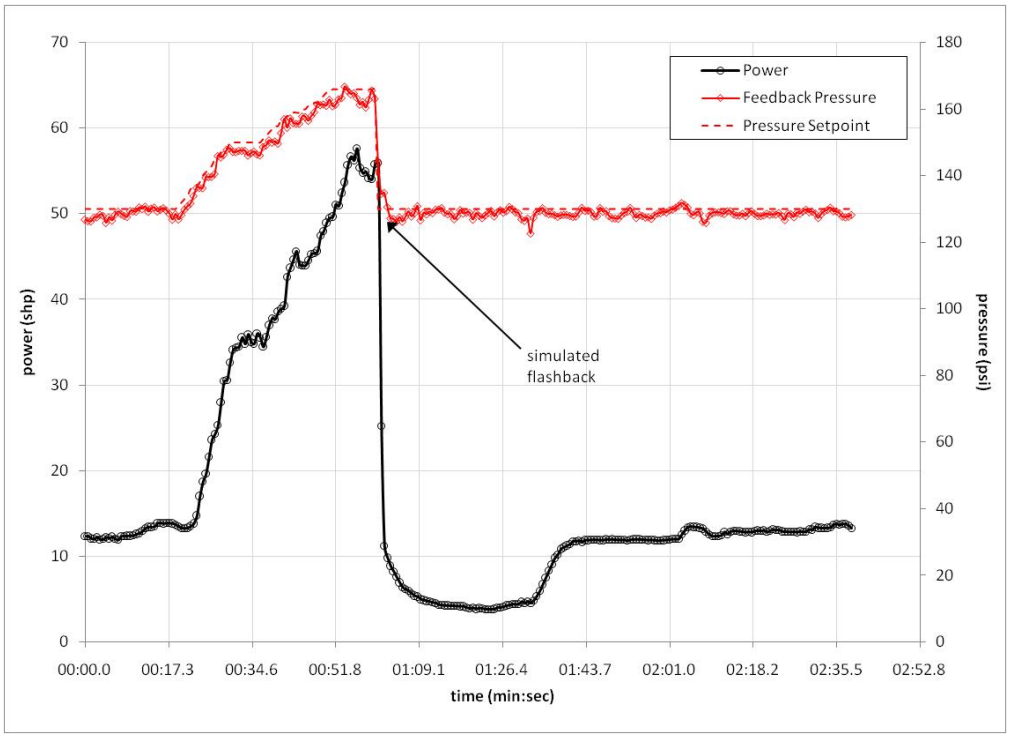

Figure 5.12. Flashback simulation during engine acceleration using analog pressure control method

Flashback during operation

During the testing phase of a redesigned combustor, a series of flashbacks occurred at similar power levels as those seen in the previous combustor design. While this was unexpected, the controller did operate as designed when a premixer shell temperature rose higher than the flashback temperature threshold. A time plot of two of such flashbacks is shown in Figure 5.13. As the serial pressure setpoint slowly increased, so did the power level of the engine. Upon reaching power levels of approximately 150 and 175 shp a flashback occurred in one of the premixers and the engine was immediately returned to idle after the premixer's bank was closed. At idle, the bank associated with the premixer that incurred the flashback was reopened to prevent the premixers from operating at a higher equivalence ratio.

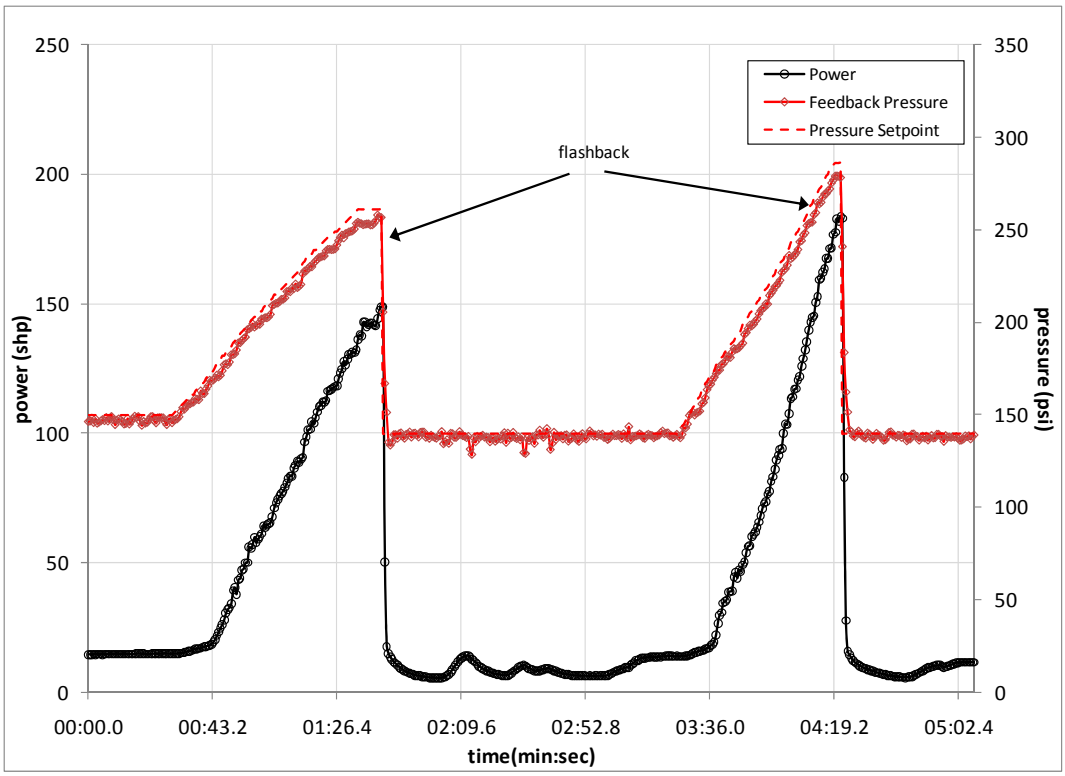

Figure 5.13. Flashback control logic activated during testing of 14-premixer design

5.3.3 Automated Operations

Ignition

After the priming sequence, the automatic ignition sequence was initiated with the opening of Bank 2. A pressure drop was seen when Bank 2 opened because the fuel manifold had initially been dead-ended. The electronic regulator compensated for this and maintained the idle pressure during the remainder of the ignition sequence. When the premixers associated with Bank 2 ignited, the average of the T_4 temperatures increased, triggering the remaining premixer banks to open in succession (with the exception of Bank 5 because of lean blowout concerns). The temperatures of the T_4 probes and fuel pressure during the ignition sequence are shown in Figure 5.14. Fuel pressure and hydrogen mass flow during this process is shown in Figure 5.15. A slightly faster response time of only one T_4 probe during ignition suggests that the probe was directly in the flow stream of one of the three premixers associated with the ignition of Bank 2. The engine experienced a near-step change in fuel flow during ignition, indicated by the sudden rise in fuel flow and rise in T_4.

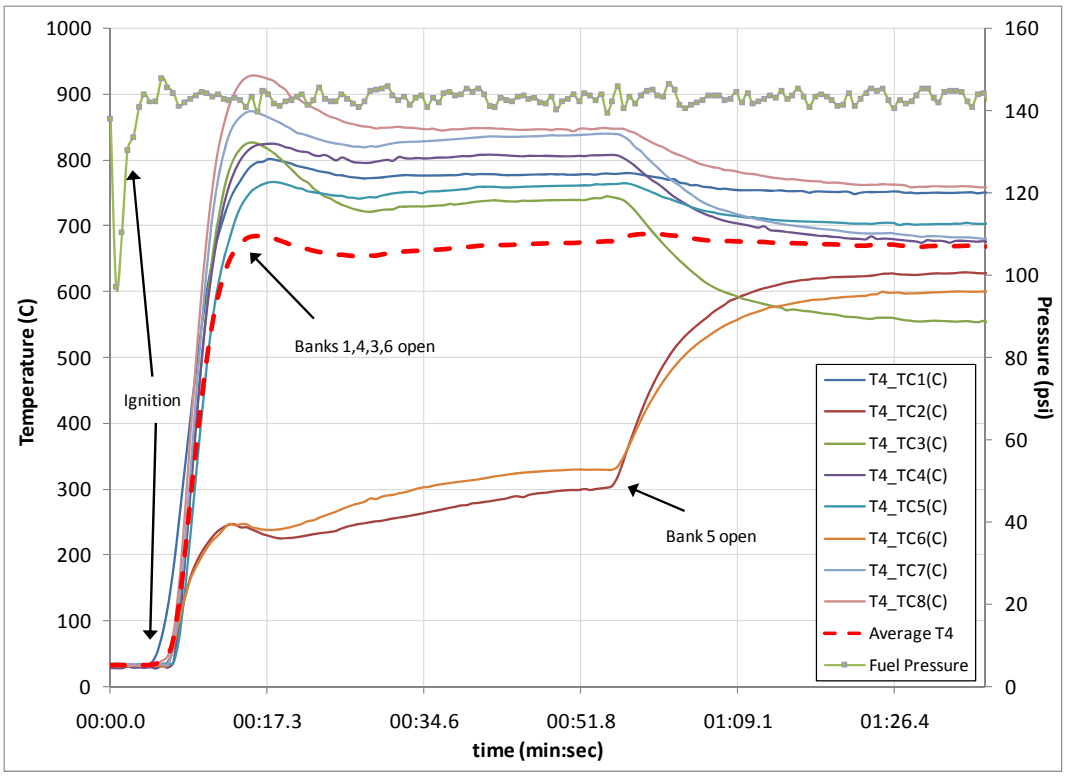

Figure 5.14. Ignition sequence showing fuel pressure and T_4 response

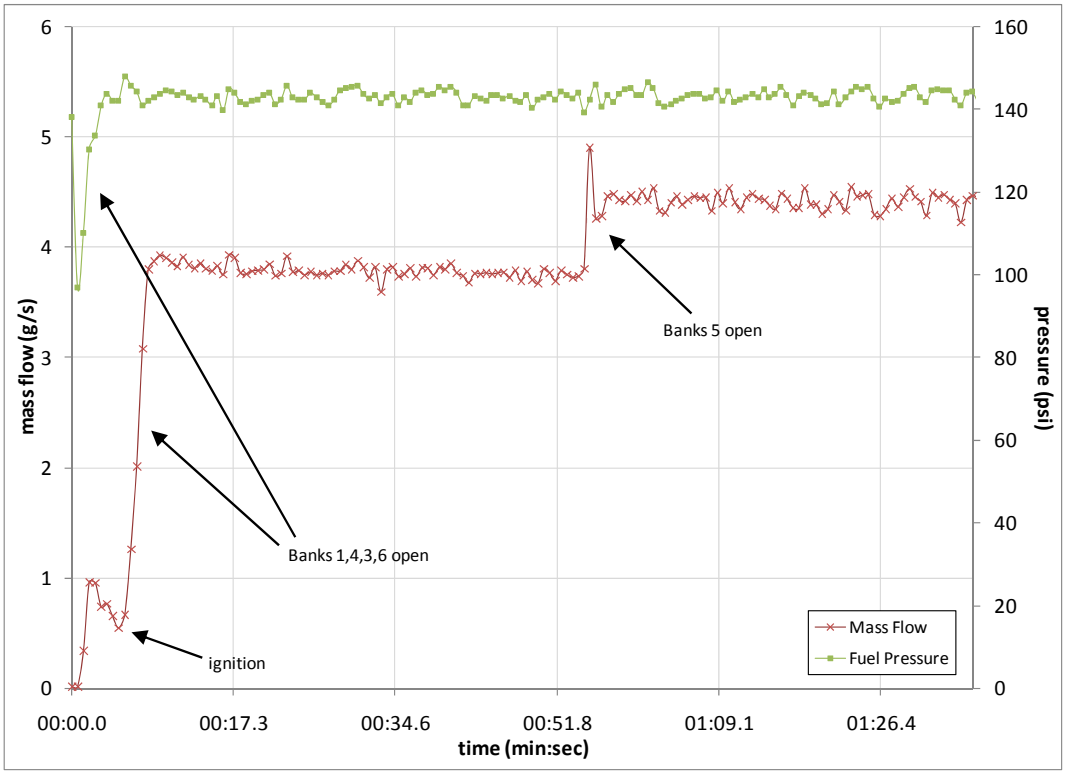

Figure 5.15. Ignition sequence showing fuel pressure and increase in fuel mass flow

Locally, the equivalence ratio was relatively rich until the opening of Bank 5. Until Bank 5 was open, all but two T_4 probes showed temperatures indicative of combustion. The two probes failed to register the same increase in combustor outlet temperature because the probes were in the vicinity of a premixer associated with Bank 5, as shown in Figure 3.3b. After the opening of Bank 5, the engine remained at idle until all premixers reached approximately a steady-state temperature and the experiment was allowed to continue. The variation in measured T_4 levels without and with Bank 5 activated indicated little mixing of the individual injector flow streams in the burner quench zone. This was an undesirable characteristic, possibly due to the reduced combustion gas quench volume caused by the volume occupied by the fuel premixers.

Hydrogen purge

As part of the overall shutdown procedure, the hydrogen purge sequence occurred after ITT decreased below 100 ^{o}C to prevent cool N_2 quenching of the engine hot section. A plot of a normal purge sequence is shown in Figure 5.16. The pressure was held constant until ITT decreased to the appropriate temperature. During the process shown in Figure 5.16, cooling was accelerated by turning the engine starter on and allowing air to flow through the engine. As ITT fell, it triggered the start of the purge sequence as it dropped below 100 ^{o}C. All premixer banks were open and N_2 flowed through the system for ten seconds, both downstream of the purge valve through the engine as well as upstream and out of the open bleed valve. When the purge sequence ended, the starter was turned off ($\%N_g = 0$) and the engine returned to its safe non-operational state.

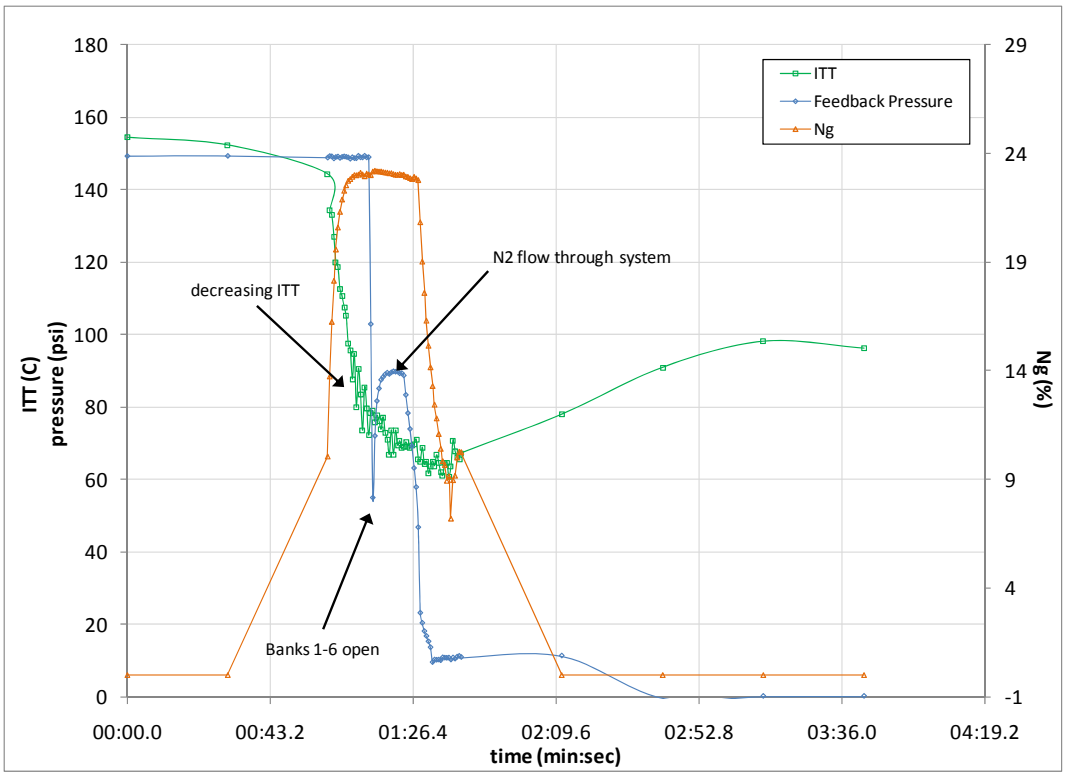

Figure 5.16. Purge sequence after shutdown.

5.4 Discussion of Results

Each function of the fuel controller (with the exception of high ITT) was successfully tested during engine operation. While some of the control methods and functions did not have a full range of tests, the experiments that were performed demonstrated the ability of the fuel control system to take appropriate actions within the limitations of both the control logic and engine operability. By design, some of the programmed functions of the fuel controller can be modified during engine operation to test engine operability beyond that seen from experience. For example, the flashback threshold can be increased to a temperature higher than that of the default value, or $\frac{dP_{fuel}}{dt}$ can be increased to test the transient operation of the engine to a desired power setting. Future iterations of the controller and combustor design may see an increase in engine operability and fuel control system capability.

Chapter 6: Approaches to Modeling and System Identification

This chapter focuses on techniques for system identification, or experimental modeling, of the PT6A-20 using power output as a function of fuel pressure setting. Engine models and simulations are often created during the engine development process; however, these models are often proprietary to the manufacturer, making efficient fuel control design for modified engines difficult. The addition of the digital fuel controller to this system allows new experiments to be designed and implemented for determining the characteristics of the engine. These characteristics can be modeled to predict the performance of the engine and ultimately the models can be incorporated to the fuel control logic for better control performance. An excellent summary of different modeling methods for gas turbine engines is presented by Kulikov and Thompson in *Dynamic Modelling of Gas Turbines: Identification, Simulation, Condition Monitoring, and Optimal Control* [26].

The first section of this chapter briefly introduces an approach to analytical modeling of gas turbine engines. This is followed by an overview of system modeling in the time and frequency domains using sampled test data. Input signals that produce sufficient data for engine modeling are summarized in the subsequent section. The chapter concludes with a time-domain model based on PT6A-20 test data from idle to 100 shp.

6.1 Mathematical Modeling

Simplified thermodynamic models are part of the first steps of both engine and controller design. With knowledge of numerical values of key engine variables, nonlinear static and nonlinear dynamic models can provide the starting point of the design process [26]. Static models that

represent fuel scheduling characteristics are incorporated into the preliminary design of the fuel controller. Dynamic modeling considers the transients of the engine when operating at off-design points. A good example case in which such a simulation was successfully created was presented in 1999 by Lin et al [27]. A dynamic simulation of a single spool turbojet engine was generated that was solved using different integration methods to compare computing times. The differential equations were derived from the fundamental equations (mass conservation, momentum, energy, etc.) and solved using a hybrid explicit-implicit integration method. The governing equations for the turbojet simulation would provide a good foundation for creating a model of the PT6A-20.

The first iteration of the controller is tested with the simulated engine to define a static operating line. Data from these tests as well as tests from the physical engine are used to refine the models and the process is repeated until simulation and controller performance is satisfactory. A technique for evaluating the effect of the controller on the simulation is to express the system in state-space form. Using this method in 1989, Kulikov represented a single-shaft gas turbine with static and dynamic mathematical models [28]. These models can be applied to the PT6A-20 or any other gas turbine engine to create a starting point for a fuel control map. Adapting the static model for the PT6A-20, the engine representation has the form

$$\begin{cases} \boldsymbol{f_x}(\boldsymbol{X}, \boldsymbol{U}, \boldsymbol{V}) = \boldsymbol{0} \\ \boldsymbol{Y} = \boldsymbol{f_y}(\boldsymbol{X}, \boldsymbol{U}, \boldsymbol{V}) \end{cases}$$

Equation 6.1

where

$\boldsymbol{X} = \left[\dot{m}_a, \dot{m}_f, T_4, ITT\right]^T$ is the state vector that describes steady-state configuration of the engine;

$\boldsymbol{U} = \left[\dot{m}_f\right]$ is the control (input) vector;

$\boldsymbol{V} = [M, p_{atm}, T_{atm}]^T$ is the atmospheric conditions vector; and

$\boldsymbol{Y} = \left[\frac{N_g}{\sqrt{\theta}}, P_{03}, \frac{P_{0_3}}{P_{0_2}}, \ldots\right]^T$ is the observed coordinates (output) vector.

The state vector $\boldsymbol{X}$ could have any number of variables that appropriately describe the engine at steady-state. The dynamic engine model has the state space form

$$\begin{cases} \dot{\boldsymbol{X}} = \boldsymbol{F_x}(\boldsymbol{X}, \boldsymbol{U}, \boldsymbol{V}) \\ \boldsymbol{Y} = \boldsymbol{F_y}(\boldsymbol{X}, \boldsymbol{U}, \boldsymbol{V}) \end{cases}$$ **Equation 6.2**

and includes the differential equations describing transient characteristics of the engine. At steady-state, $\boldsymbol{F_x}$ and $\boldsymbol{F_y}$ reduce to $\boldsymbol{f_x}$ and $\boldsymbol{f_y}$. The dynamic equations include changes in fuel pressure or flow, air properties with respect to speed and altitude, and changes in shaft speed. Derivations of some of these differential equations with knowledge of off-design performance can be found in *Gas Turbine Theory* by Cohen and Rogers or *Mechanics and Thermodynamics of Propulsion* by Hill and Peterson[29][9].

As an example of how to find the relationship between fuel flow and gas generator (rotor) speed, the net power generated is first examined since it can be related to the rate of change of compressor rotor speed. This relationship is expressed as

$$\dot{n} = \frac{\mathcal{P}_t - \mathcal{P}_c}{Jn\left(\frac{\pi}{30}\right)^2}$$ **Equation 6.3**

where $\mathcal{P}_t$ is the turbine power, $\mathcal{P}_c$ is the compressor power, J is the polar moment of inertia of the compressor rotor, and n is the shaft speed. Relating the power to increments in fuel flow can be done by considering the off-design performance presented in a compressor map and a turbine map. While the compressor map may be unknown at this point in the design process, off-design points picked off an existing map can be used for estimation and scaled accordingly with the preliminary model. Iterating with different compressor maps would help to refine the analytic model. A schematic of a general turbojet engine is shown in Figure 6.1. Each station on the diagram represents a different process within the engine.

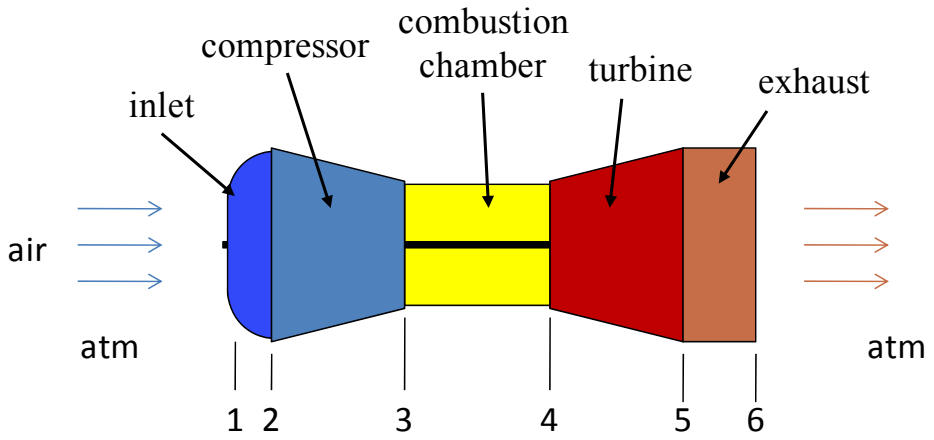

Figure 6.1 Diagram of a gas turbine engine

Using the stagnation properties at each of the stations in Figure 6.1, the flow relationship between the compressor and turbine is given as

$$\frac{\dot{m}_a\sqrt{T_{04}}}{P_{04}} = \left(\frac{\dot{m}_a\sqrt{T_{02}}}{P_{02}}\right)\left(\frac{P_{02}}{P_{03}}\right)\left(\frac{P_{03}}{P_{04}}\right)\left(\sqrt{\frac{T_{04}}{T_{02}}}\right) \qquad \textbf{Equation 6.4}$$

With a design point from the turbine and compressor maps, the turbine inlet temperature can be determined. Rearranging Equation 6.4 gives

$$\sqrt{\frac{T_{04}}{T_{02}}} = \left[\frac{\dot{m}_a\sqrt{T_{04}}}{P_{04}}\left(\frac{P_{03}}{P_{02}}\right)\left(\frac{P_{04}}{P_{03}}\right)\right] \Big/ \frac{\dot{m}_a\sqrt{T_{02}}}{P_{02}} \qquad \textbf{Equation 6.5}$$

Since $\dot{m}_a$, T_{03}, and T_{04} are now assumed known, fuel flow for T_{04}/T_{02} can be calculated from

$$f = \frac{\frac{T_{04}}{T_{03}} - 1}{\frac{Q_R}{c_p T_{03}} - \frac{T_{04}}{T_{03}}} \qquad \textbf{Equation 6.6}$$

where f is the burner fuel-air ratio and Q_R is the heat of reaction. A more detailed derivation of the fuel-air ratio is given in the appendix. Finally, the power produced by the turbine is given as

$$\mathcal{P}_t = \eta_t\left(\dot{m}_a + \dot{m}_f\right)c_{p_{f-a}}\Delta T_{045} \qquad \textbf{Equation 6.7}$$

with

$$\Delta T_{045} = \left(\frac{\Delta T_{045}}{T_{04}}\right)\left(\frac{T_{04}}{T_{02}}\right)(T_{02}) \qquad \textbf{Equation 6.8}$$

The compressor power is calculated as

$$\mathcal{P}_c = \dot{m}_a c_{p_a} \Delta T_{023} \qquad \textbf{Equation 6.9}$$

and the change in shaft speed of the rotor for a *single* turbine operating point is

$$\dot{n} = \frac{1}{Jn\left(\frac{\pi}{30}\right)^2}\left[\eta_t\left(\dot{m}_a + \dot{m}_f\right)c_{p_{f-a}}\Delta T_{045} - \dot{m}_a c_{p_a}\Delta T_{0_{23}}\right] \qquad \textbf{Equation 6.10}$$

where

J is polar moment of inertia of the rotor;
n is the shaft speed
η_t is the efficiency of the turbine;
$\dot{m}_a$ is the mass air flow;
$\dot{m}_f$ is the mass fuel flow;
$c_{p_{f-a}}$ is the specific heat at constant pressure of the fuel/air mixture;
$\Delta T_{0_{45}}$ is the change in total temperature of the turbine;
c_{p_a} is the specific heat at constant pressure of the air; and
$\Delta T_{0_{23}}$ is the change in total temperature of the compressor.

A series of turbine operating points creates a transient line that shows the dependency of compressor speed on fuel flow. By iterating with different (scaled) component maps, the model converges to the actual transient line of the engine. Similar transient lines of other engine characteristics can be made using different thermodynamic relationships that can be represented in the state-space form of Equation 6.2.

6.2 System Identification Techniques

Experimental modeling of the modified PT6A-20 has two advantages, one being that the performance of the engine can be predicted and compared to that of Jet-A operation using actual engine data and the other advantage that the predicted performance can be integrated into the fuel control design. For the PT6A-20, linear modeling is used for describing the engine dynamics at steady-state operating points. In general, transient performance is harder to describe because of the nonlinear properties associated with the engine, such as air properties, and component properties due to thermal changes (for example blade tip clearances) and shaft speed.

Several studies have been performed to model the transients of an engine. For example, a 1996 investigation by Grose attempted to identify the transient response of gas turbine components using time-domain analysis by combining steady-state engine data with transient data [30]. Inclusion of nonlinear properties into the linear modeling can account for these variations during transients.

For modeling the performance of the modified PT6A-20, the system (or plant) H is assumed to be the engine, pressure regulator, and dynamometer with the input to the system being the digital fuel pressure setpoint and the output the calculated shaft power. A modified block diagram of Figure 4.5 is shown in Figure 6.2, with the system described in the dashed box. The control loops of the electronic regulator and the dynamometer were included because the power would be controlled by varying the pressure setpoint and measuring the applied torque and shaft speed for calculating the shaft power. System identification of the system in Figure 6.2 can be performed in either the time domain or the frequency domain.

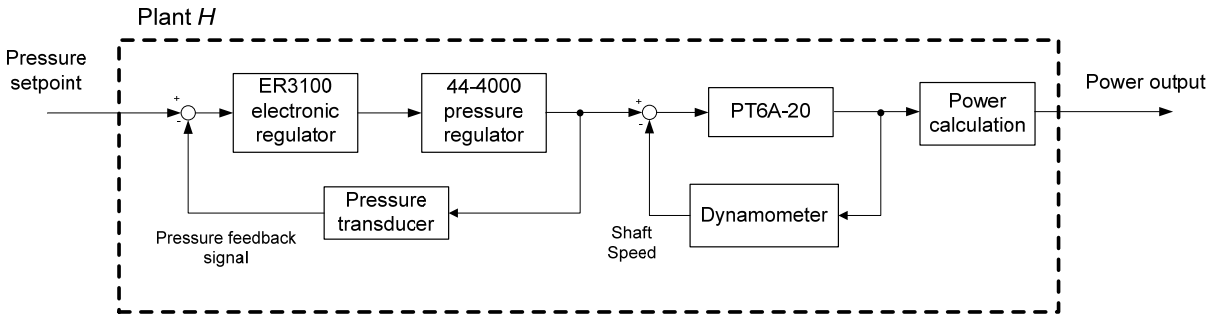

Figure 6.2. Block diagram of system structure used for modeling

Time domain characterization can be determined from the impulse response once the engine has reached steady-state, and can be described by the convolution of the input and impulse response

$$y(t) = \int_{\tau=0}^{\infty} h(\tau)u(t-\tau)d\tau = h(\tau) * u(\tau) \qquad \tau \geq 0 \qquad \textbf{Equation 6.11}$$

where $u(\tau)$ is the input to the system, $y(t)$ is the output, and $h(\tau)$ the unit impulse response. Because the data is sampled, analysis is performed in the discrete time (z) domain with the ability to be converted to the continuous time (s) domain assuming a zero-order hold (ZOH) using the conversion

$$z = e^{sT_s} \qquad \textbf{Equation 6.12}$$

Equation 6.11 in the z-domain is given as

$$y(kT_s) = \int_{\tau=0}^{t} h(\tau)u(kT_s - \tau)d\tau, \quad k = 1,2,\ldots \qquad \textbf{Equation 6.13}$$

where T_s is the sampling interval. Linear model estimation in the discrete time z-domain can be obtained using one of the methods in Table 6.1:

Table 6.1. Models used for system identification in the time domain

Auto Regressive with eXogenous input (ARX)	Easiest to implement, estimation using auto regression; disadvantage: may be higher order than necessary to account for noise input in the model
Auto Regressive Moving Average with eXogenous input (ARMAX)	Allows flexibility of changing parameters for the noise input model
Output Error (OE)	Models only the system dynamics
Box-Jenkins (BJ)	"Complete model" that separately models the system dynamics and noise

Ljung and Glad describe in detail the advantages of and the differences among these and other model structures in *Modeling of Dynamic Systems* [31]. The decision to use one model over another depends on how well the model fits existing data and how well new data matches the model.

Frequency domain analysis is another method for identifying a model for an unknown system. A model for frequency domain identification based on the modified PT6A-20 "plant", including error associated with the power output measurement, is shown in Figure 6.3. In the diagram, $u(s)$ is the input pressure setpoint at a specified frequency and $y(s) = \hat{y}(s) + n(s)$ is the power output at the same frequency plus measurement noise. Since the input is the pressure setpoint and not the measured pressure output, the noise of the pressure regulator output is incorporated within the plant, H. The same is true for the torque and shaft speed measurements acquired by the dynamometer.

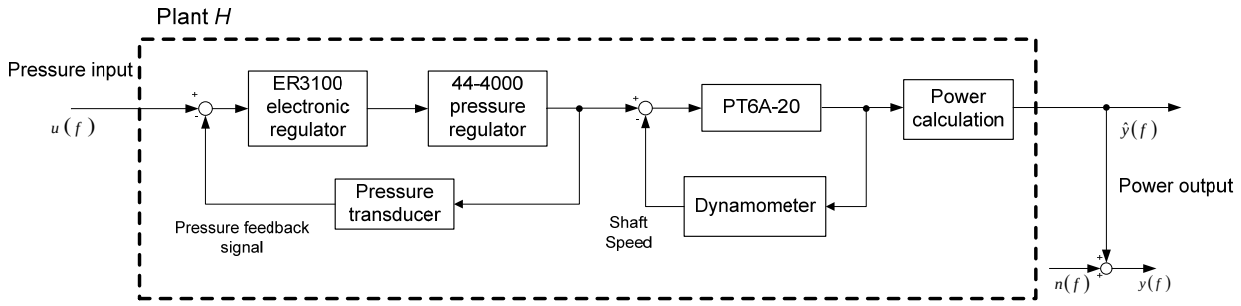

Figure 6.3. Pressure regulator-engine structure used for system identification in the frequency domain

The frequency response function (FRF) at a steady-state design point of the system shown can be determined by taking steady-state data in an experimental manner as described in the next section. The estimators H_1 and H_2 are bounds for the true transfer function, H_{true}, and are given as

$$H_1 = \frac{G_{uy}}{G_{uu}} \qquad \textbf{Equation 6.14}$$

$$H_2 = \frac{G_{yy}}{G_{yu}} \qquad \textbf{Equation 6.15}$$

$$|H_1| \leq |H_{true}| \leq |H_2| \qquad \textbf{Equation 6.16}$$

where G_{uy} and its complex conjugate G_{yu} are cross spectra of the data. The auto spectra of the input and output are G_{uu} and G_{yy}, respectively. It is of note that the output signal contains noise that can be quantified by the coherence function,

$$\gamma^2 = \frac{|G_{uy}|}{G_{uu}G_{yy}} \qquad \textbf{Equation 6.17}$$

A coherence value of one at a specific frequency indicates that the engine power output is totally dependent on the pressure setpoint. Coherence values less than one could indicate uncorrelated noise corrupting the measurement, nonlinearities within the pressure regulator-engine system, or leakage errors occurring during the conversion of the data from the time domain to the frequency domain using a fast Fourier Transform (FFT) [26]. Influences by uncorrelated noise is minimized with more averaging (data collection). Leakage errors in the FFT can be reduced

using a windowing function. Common windowing functions include the Hamming, Hann, and Blackman windows.

6.3 Input Signals for System Excitation

As discussed in the previous section, system identification can be performed in either the time domain or the frequency domain. The system may be excited by impulse, step, or ramp inputs, random signals, and periodic signals. Impulse, step, and ramp inputs can be used for time domain identification, using the modeling techniques in Table 6.1. Problems with these signals are that they tend to suffer poor signal to noise ratios (SNR) and do not provide sufficient data for the averaging needed for accurate FRF estimation. Random signals at steady-state are ill advised for identification (especially with large amplitudes to overcome the SNR) since the responses of the engine and the premixers to the sudden pressure variations are unknown. This is also true for step and impulse inputs in which the fuel pressure suddenly increases.

A periodic signal consisting of a multisine function can be added to the fuel pressure setpoint, exciting the system at a range of frequencies. A multisine signal is a collection of cosine signals with different amplitudes, frequencies, and phases, given by

$$u(t) = \sum_{k=1}^{F} \boldsymbol{A}(k) cos[\boldsymbol{i}(k) 2\pi f_0 t + \boldsymbol{\phi}(k)] \qquad \textbf{Equation 6.18}$$

with $\boldsymbol{A}$, $\boldsymbol{i}$, and $\boldsymbol{\phi}$ the vectors of signal amplitudes, harmonic integers, and phases, respectively. The fundamental frequency, f_0, was chosen in a past study as 0.005 Hz with a bandwidth of 0.005-0.04 Hz to study the low frequency turbine dynamics [32]. It is recommended to use this method to find the FRF of steady-state design since the investigator can choose the attributes of the multisine signal using *a priori* knowledge of the engine. A downside to multisines, though, is the time required to obtain data for just one period with low frequency signals.

In the present study, the power of the engine was increased by ramping the fuel pressure to the appropriate setting. The pressure setting was ramped to avoid surging the engine and to avoid creating conditions favorable to flashbacks. A model was created from the input and output signal using the Box-Jenkins time domain structure.

6.4 System Identification from Idle to 100 shp

System identification of the modified PT6-A20 was performed using the system structure of Figure 6.2. Ideally, experimental modeling in the time domain would use engine response to an impulse or step input, or in the frequency domain would use multisines for system excitation. More information can be obtained through system identification using these techniques; however, data used for system identification in this section does, in fact, show that an empirical model can be used to describe the system shown at these operating conditions.

Three sets of data were chosen that represented a ramped increase in fuel pressure from idle to 100 shp. Model estimation was performed using the System Identification Toolbox in MATLAB 7.6. For linear parametric model estimation, one dataset was used for estimation and the model was validated with the other two sets of data. Shown in Figure 6.4 are the digital pressure setpoint and the power output of the engine.

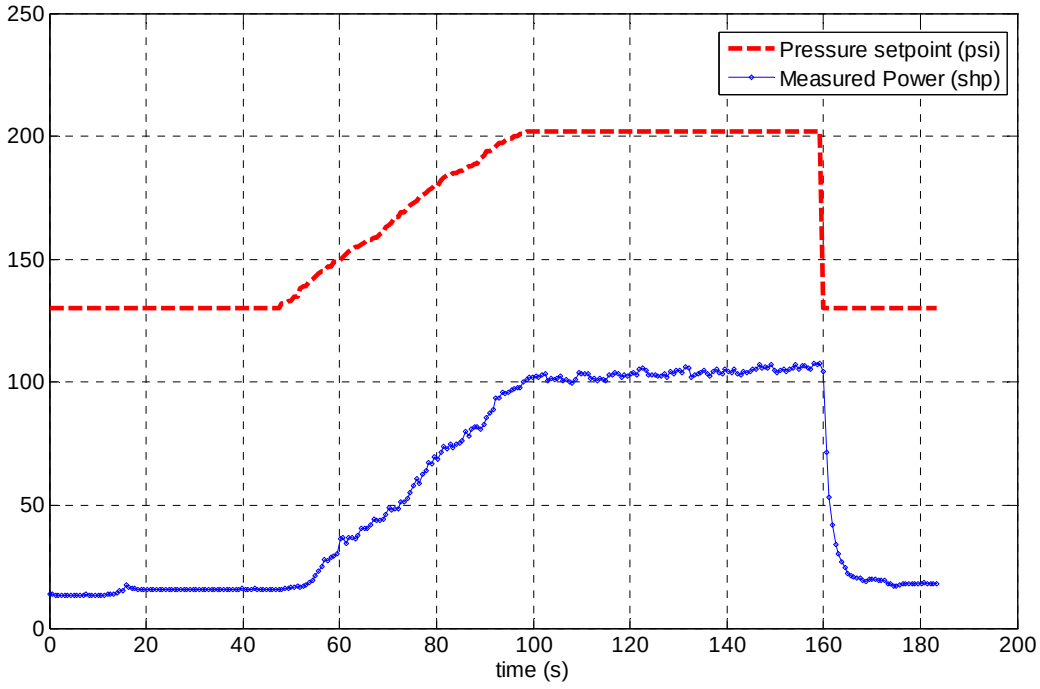

Figure 6.4 Input and output data used for model estimation

The System Identification Toolbox has several different models that can be utilized for estimating a system, including linear parametric, process, and nonlinear models. A linear parametric model was chosen for this application because the response of the engine during these

tests followed a fairly linear trend. Of the various linear models to choose from, the Box-Jenkins model was used to create the estimated model using the data from Figure 6.4 and was validated using the data in Figure 6.5.

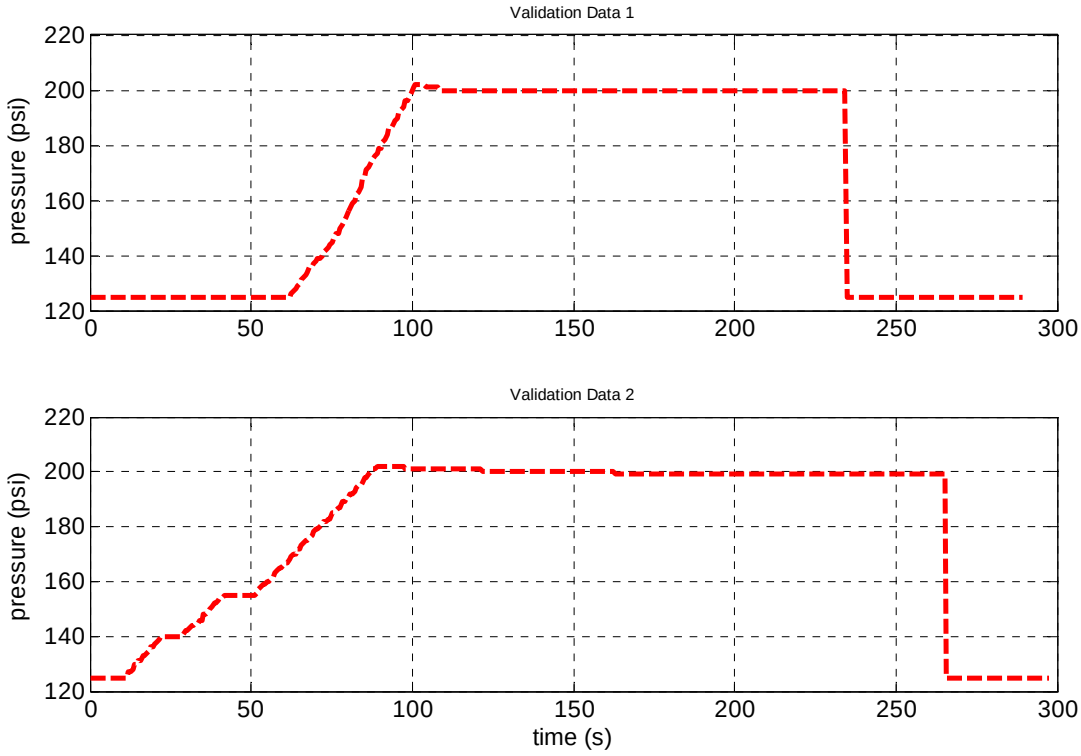

Figure 6.5. Validation data for system identification

The transfer function of the Box-Jenkins model is given in the z-domain as

$$H(z) = \frac{0.4489z - 0.4488}{z^2 - 1.592z + 0.5921} \qquad \textbf{Equation 6.19}$$

Using Equation 6.12 to convert from the z-domain to the s-domain (assuming a ZOH) gives

$$H(s) = \frac{0.91532(s + 0.0002322)}{(s + 0.8318)(s - 2.36\times10^{-8})} \qquad \textbf{Equation 6.20}$$

When compared to the validation data, the model fit the data to within approximately 87% of the experimental data. The model results and the experimental data for the two validation data sets are shown in Figures 6.6 and 6.7. The nonlinearity of the system is in evidence at the end of each time trace by a fairly large discrepancy between the model and

experimental data. This can be minimized by either applying a nonlinear model, or by normalizing the experimental data by subtracting the idle pressure (e.g. 130 psig) from the data and applying the linear black-box model. The idle pressure would have to be added back in for comparison between actual experimental data and the model.

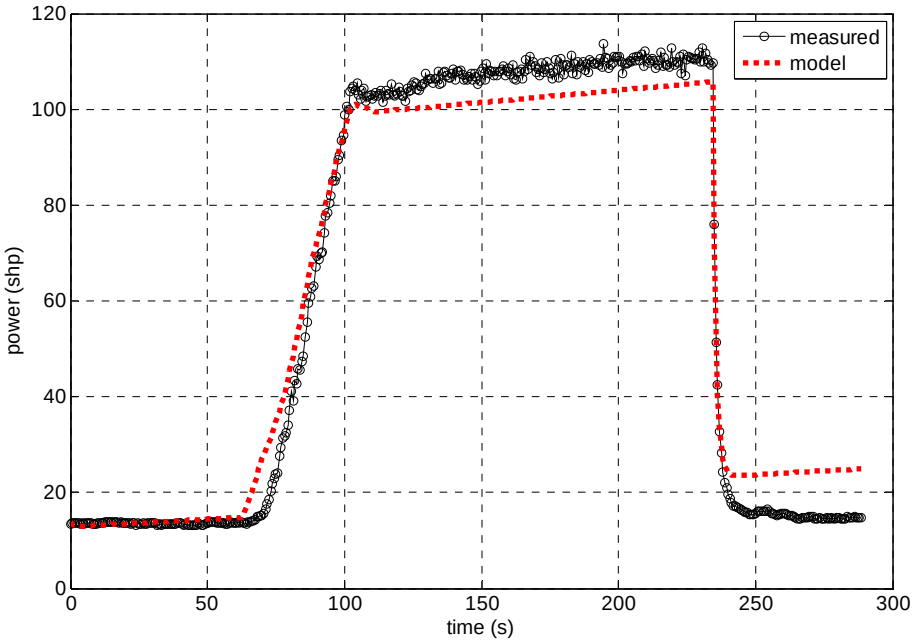

Figure 6.6 Comparison of Box-Jenkins model and engine power output for Validation Data 1 (model 86.71% accurate)

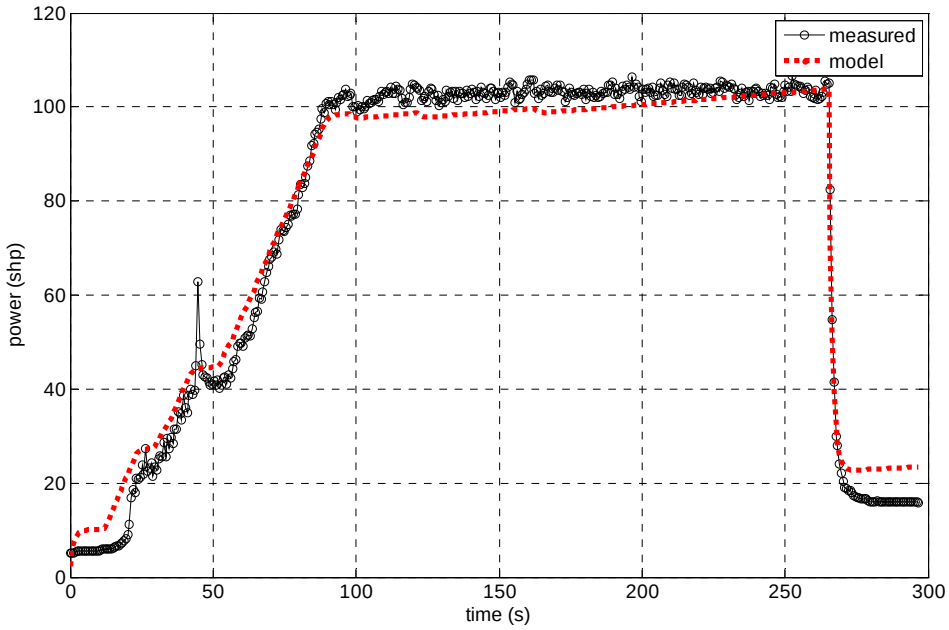

Figure 6.7 Comparison of Box-Jenkins model and engine power output for Validation Data 2 (model 87.96% accurate)

A pole-zero map of the model is shown in Figure 6.8. The pole-zero cancellation shown indicates that the model could be described as a first-order system. Classification of the engine as a low pass filter is confirmed by the pole located at s = -0.8318. Attempts to reduce the order of the system, however, resulted in a model that was far less accurate than the one chosen.

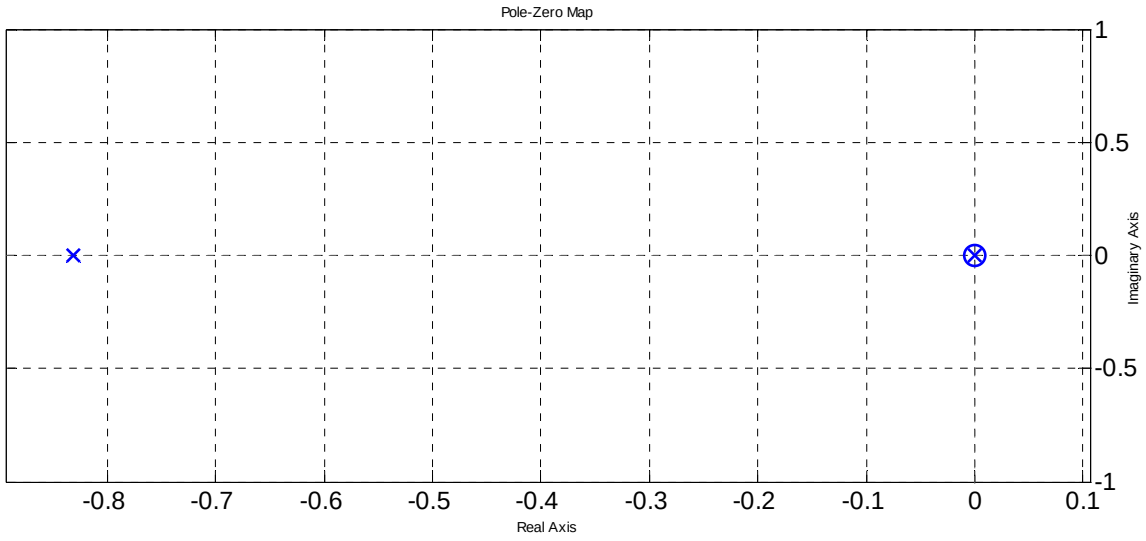

Figure 6.8. Pole-zero map of design point model

By using the system identification technique presented in this section, an experimental model can be created for several steady-state points that represent the operating range of the engine. A control map encompassing the models can be created, but the engine's transient operation would also have to be included.

6.5 Summary of Engine Modeling for Control Design

In this chapter, different methods for engine modeling for control design were discussed. Control design begins with mathematical models that are incorporated into the fuel controller and tested using the engine under development. The control model is refined with experimental data to ensure model accuracy. Modeling with engine test data is another approach with which a fuel controller can be designed. Assuming a linear system, system identification can be performed using impulse or step inputs in the time domain, or by analyzing periodic input signals and corresponding engine response. Application of nonlinear modeling techniques would be required to study the transient performance of an engine.

A model representing the power output of the engine from idle to 100 shp was created using the Box-Jenkins model. A fuel schedule for power requests for the modified PT6A-20 can be generated using a series of steady-state and transient models with system identification and included in the engine fuel control logic.

Chapter 7: Conclusions and Recommendations for Future Studies

This chapter reviews the performance of the digital fuel controller designed for a lean-premixed hydrogen fueled gas turbine engine. The first section discusses the research entailed in designing the controller for the engine used in this investigation as well as the performance of the controller and engine during normal operation. This is followed by suggestions on how to improve the fuel controller by incorporating mathematical models and models determined from experimental engine data.

7.1 Conclusions

The fuel controller for the PT6A-20 satisfactorily managed the flow of hydrogen from the supply tanks to the engine. By coupling the DAQ system with the control algorithm, the digital fuel controller was integrated into the existing fuel system. Included in the control design was the ability to safely shut down the engine in the event of an emergency through the use of either computer control or the redundant manual control.

The electronic pressure regulator effectively controlled the fuel pressure to the engine. The majority of tests occurred in an open-loop manner in which the pressure setting was managed by an operator in order to reach and maintain a power level. Two closed-loop power control tests demonstrated the feasibility of the fuel controller to not only to reach and maintain a power request, but to be adjusted to improve its response. Tuning of the power control gains could be necessary for different steady-state operating points, but the gains would have to be determined after studying more design points with the open loop system.

Operability limits of the engine associated with premixer stability, specifically flashbacks, were incorporated into the fuel controller programming. A flashback simulation and true flashbacks were automatically and successfully managed by the controller. The response time of the controller was several seconds faster than when the engine was controlled using the previous "manual" system, therefore reducing the potential damage that might be incurred from a flashback. High ITT temperature limits were also included in the fuel controller using operating temperatures found in the PT6A-20 operator's manual.

Automatic startup, ignition, and shutdown procedures were also included in the fuel controller of the PT6A-20. During startup, the fuel manifold was pressurized so that ignition could occur with the opening of a premixer bank. A rise in T_4 indicated ignition, at which point the remaining premixers were sequentially opened. Shutdown occurred when the engine was at idle, cutting off the hydrogen supply and purging the fuel lines with nitrogen through a series of timed valve actuations.

Several techniques for modeling the engine were presented, with a focus on experimental methods. Mathematical models can provide a good start for the design of the fuel controller; however there are times when the models do not accurately describe all the dynamics of the engine. Combined with experimental data, models can better describe the steady-state and transient operation of the engine.

7.2 Recommendations for Future Studies

During the programming, testing, and analysis of this investigation, several aspects of the fuel controller were seen to have opportunities for improvement. Recommendations for continuing the investigation in this digital fuel controller design are given in order of assumed feasibility:

- The power control method was designed to conservatively reach a power request by comparing the setpoint to feedback measurements. The operator had the capability of controlling the rate at which the fuel pressure changed during engine tests, changing as the pressure measurements came closer to the setpoint. The Control Design and Simulation Toolkit in LabVIEW version 8.6 has the capability of implementing a PID control subVI. This tool uses the desired setpoint, measurement feedback, and PID gains as inputs and

outputs the signal necessary to obtain the setpoint. A more refined power control could be executed by using the PID control subVI. The PID gains could be scheduled according to the models created using system identification at different design points.

- Assuming complete range of operability of the redesigned premixers, a "bank management" scheme should be used to ensure lean blowout does not occur. By using laboratory data that characterizes the premixers according to fuel flow and air flow, the premixer banks can be turned on and off using predicted equivalence ratios. Having banks of premixers closed during operation, especially at idle and low power levels, results in the remaining premixers burning locally richer and therefore adding margin to the lean stability limits. At higher power levels all banks of premixers would be open and the engine would be able to operate to its rated 550 shp while the premixers burned at the designed equivalence ratio.

- A study could be performed on the effects of relighting the premixers after a flashback has occurred without returning to idle. Assuming this procedure was successful the engine could be kept at a specified power level, or slightly lower power level, while the fuel controller takes the appropriate measures to close and reopen the bank with the premixer that incurred the flashback.

- Experimentally, a fuel schedule for the engine can be determined and incorporated into the controller. The fuel schedule determines the appropriate rate of fuel delivery to the engine according to power request and rate of acceleration or deceleration. Fuel would be metered to the combustor at a rate to avoid combustor instabilities, compressor surge, high turbine gas temperatures, or compressor overspeed. Determining the fuel control map could occur parallel to investigating the steady-state or transient performance of the engine.

- Investigation into the surge margin is another area of research that could be performed when creating a fuel schedule. Past studies have shown that the compressor surge line can be measured by applying a fuel spiking signal to the fuel controller demand signal [33]. By using the fuel controller presented in this thesis, a fuel spike could be applied, with the

results from the test used for predicting the surge margin. The sampling rate of the DAQ would have to be increased to properly record the engine response to the fuel spike.

- Finally, an aerothermal performance model of the engine could be created for the design of future iterations of the fuel controller as well as the development of future hydrogen-modified combustors. Experimentally, this would entail numerous engine tests and a detailed model may not be feasible. The numerous equations involved in mathematically representing the static and dynamic behavior of the engine could be just as difficult. However, a model provides insight into the performance of the engine and an efficient fuel controller could be designed accordingly. Engines that are designed and prototyped have various levels of component testing that is included in engine models. During this phase, analytical and experimental data are combined to create the aerothermal model that is vital to the generation of the control map.

References

[1] Turns, S.R., *An Introduction to Combustion: Concepts and Applications, 2nd ed* (Boston, MA: McGraw-Hill, 2000).

[2] Brewer, G.D., *Hydrogen Aircraft Technology* (Boca Raton, FL: CRC Press, 1991).

[3] Marek, C.J., Smith, T.D., and Kundu, K., "Low Emission Hydrogen Combustors for Gas Turbines Using Lean Direct Injection," (AIAA-2005-3776), *41st AIAA/ASME/SAE/ASEE Joint Propulsion Conference & Exhibit*, Tucson, AZ, 2005.

[4] Odgers, J., and Kretschmer, D., *Gas Turbine Fuels and Their Influence on Combustion*, Energy and Engineering Science Series (Tunbridge Wells, Kent: Abacus Press, 1986).

[5] Brand, J. et al, "Potential Use of Hydrogen in Air Propulsion," (AIAA 2003-2879), *AIAA/ICAS International Air and Space Symposium*, Dayton, Ohio, 2003.

[6] Rajagopalan, R., Wood, B.C., and Schryver, M., "Evolution of Propulsion Controls and Health Monitoring at Pratt and Whitney," (AIAA 2003-2645), *AIAA/ICAS International Air and Space Symposium and Exposition*, Dayton, Ohio, 2003.

[7] Mattingly, J.D., Heiser, W.H., and Pratt, D.T., *Aircraft Engine Design*, 2nd ed., AIAA Education Series (Reston, VA: American Institute of Aeronautics and Astronautics, 2002).

[8] Hill, P. and Peterson, C., *Mechanics and Thermodynamics of Propulsion, 2nd ed* (Reading, MA: Addison-Wesley, 1992).

[9] Keck, M.F., Fredlake, J.J., and Schwent, G.V., "A Control Concept Combining the Best of the Current and Hydromechanical Electronic Technologies," SAE Paper 740380, 1974.

[10] Jaw, L.C., and S. Garg, *Propulsion Technology Development in the United States: A Historical Prospective,* NASA/TM-2005-213978 (Cleveland, OH: NASA Glenn Research Center, 2005).

[11] Giampaolo, T., *Gas Turbine Handbook: Principles and Practices, 3rd ed* (Lilburn, GA: Fairmont Press, 2006).

[12] Adibhatla, S., and H. Brown, "Intelligent Engine Control (IEC), (AIAA 92-3484), *28th AIAA/SAE/ASME/ASEE Joint Propulsion Conference and Exhibit*, Nashville, TN, 1992.

[13] Behbahani, A., et al, "Multi-Core Processors: An Enabling Technology for Embedded Distributed Model-Based Control," (AIAA 2008-5275), *44th AIAA/ASME/SAE/ASEE Joint Propulsion Conference & Exhibit*, Hartford, CT, 2008.

[14] Sloop, J.L., *Liquid Hydrogen as a Propulsion Fuel, 1945-1959*, NASA SP-4404 (Washington, D.C.: NASA History Office, 1978).

[15] Sosounov, V., and V. Orlov, "Experimental Turbofan Using Liquid Hydrogen and Liquid Natural Gas as Fuel," (AIAA 90-2421), *26th AIAA/SAE/ASME/ASEE Joint Propulsion Conference*, Orlando, FL, 1990.

[16] Ford, A.E., "Hydrogen-Fueled Turbine Boat Demonstration," SAE paper 770797, 1977.

[17] Therkelsen, P. et al, "Analysis of NO_x Formation in a Hydrogen-Fueled Gas Turbine Engine," *Journal of Engineering for Gas Turbines and Power*, vol. 131, no. 3 (2009), 031507 (10 pages).

[18] Perry, M.V., *An Investigation of Lean Premixed Hydrogen Combustion in a Gas Turbine Engine*, Virginia Tech: Blacksburg, 2009.

[19] Homitz, J., *A Lean-Premixed Hydrogen Injector with Vane Driven Swirl for Application in Gas Turbines*, Virginia Tech: Blacksburg, 2006.

[20] *Guide to Safety of Hydrogen and Hydrogen Systems*, ANSI/AIAA G-095-2004 (Reston, VA: American Institute of Aeronautics and Astronautics, 2005).

[21] *ER3000 Electronic Pressure Controller – User Manual*, Tescom Form #1893 (Elk River, MN: Tescom, 2007).

[22] Ogata, K., *System Dynamics, 2nd ed* (Upper Saddle River, NJ: Prentice Hall, 2004).

[23] *PT6A-20 Series Turboprop – Training Manual*, Pratt & Whitney Canada (Canada: Pratt & Whitney Canada, Inc, 1999)

[24] Phelan, R. M., *Automatic Control Systems* (Ithaca, NY: Cornell University Press, 1977).

[25] Anderson, W., *Controlling Electrohydraulic Systems* (New York, NY: CRC Press, 1988).

[26] Kulikov, G.G. and Thompson, H.A., *Dynamic Modelling of Gas Turbines: Identification, Simulation, Condition Monitoring, and Optimal Control*, Advances in Industrial Control Series (London, England: Springer, 2004).

[27] Lin, S. et al, "Real-Time Dynamic Simulation of Single Spool Turbojet Engines," *Simulation*, vol. 73, no. 6 (1999), pp. 352-361.

[28] Kulikov, G.G., "Dynamic characteristic of a gas turbine", *Optimization of Multivariable Control Systems of Aero Gas Turbine Engines* (Moscow, Russia: Mashinostroenie, 1989).

[29] Cohen, H. and Rogers, G.F., *Gas Turbine Theory, 4th ed.* (Harlow, England: Addison-Wesley-Longman, 1996).

[30] Grose, M.D., *A System Identification Technique for Predicting Transient Operation of Gas Turbine Engines*, Virginia Tech: Blacksburg, 1996.

[31] Ljung, L. and Glad, T., *Modeling of Dynamic Systems* (Englewood Cliffs, NJ: Prentice Hall, 1994).

[32] Borrell, A., Evans, C., and Rees, D., "Identification of Aircraft Gas Turbine Dynamics Using Frequency-Domain Techniques," *Control Engineering Practice, 8*, pp. 457-467, 2000.

[33] Lee, J. et al, "Surge Line Measurement of a Gas Turbine Engine by Fuel Spiking Test," (AIAA 2005-810), *43rd AIAA Aerospace Sciences Meeting and Exhibit*, Reno, NV, 2005.

Appendix

Table A.1 ER3100 Series specifications for ordered part ER3100SI-1 [21]

Enclosure	NEMA 4X
Media	Dry instrument grade air or nitrogen
Inlet Pressure	Minimum: Outlet pressure + 1 psig Maximum: 120 psig Typical: 110psig
Environment	**Temperature** -30°C to 75°C (dry nitrogen supply gas) -20°C to 60°C (KEMA Explosion Proof Versions M & N) 5°C to 75°C (Shop air) **Pressure** 28 – 32 inches Hg **Humidity** To 100% R.H. (non-condensing) @ 0°C to 75°C
Flow Rate	Cv: 0.01
Power Requirement	Voltage: 24V (22V to 28V) Current: 340mA Max, 180mA nominal
RS485 Communication Interface	Networking: Up to 32 controllers on one network Cable length: 4000 ft. max Baud rate: 9600
Accuracy	Room temp.: 0.1% of span max Temp. effects: 0.002%/°F of span max.
Response Time	Rise Time: 257ms – 10 psi to 90psi Fall Time: 552ms – 90 psi to 10psi *Note: step response into dead-end system (1 cubic inch volume)*
Ports	Conduit: 1/2" NPT Pneumatic: 1/8" NPT – Inlet, exhaust and gauge ports 1/4" NPT – Controlled outlet port
Weight	34.8 oz (1.0 kg)
External Analog Input Impedance	4-20mA: 250Ω 1-5V: 220 KΩ – Single Input Pin to Ground 1.7 MΩ – Differential input
Digital Outputs	Current: 50mA continuous, 100mA instantaneous Voltage: 5V – 28V Type: Open collector, grounded emitter
Digital Inputs	**Voltage Range/Input Impedance** 4-20mA: 250Ω 1-5V: 220 KΩ – Single Input Pin to Ground 1.7 MΩ – Differential input **Type** Level sensitive
Analog Output	4-20mA: 0.5% accuracy
Sensor Update Rate	25ms: rate of sensor reading and processing task

Table A.2 44-4000 Series specifications for ordered part 44-4012E208ER042

Basic Series	44-40
Body Material	Brass
Maximum Bias Pressure	200 psig
Soft Goods	O-ring: Viton® Seat: CTFE Gasket: CTFE Temperature: 0°F to 165°F (-17°C to 73°C)
In and Out port type	NPT
In and Out port size	1/2”
Other	750psig outlet, Cv = 0.7

Table A.3 PT6A-20 operating limits [23]

Condition	Operating Limits								
Power Setting	SHP	Torque		ITT °C (°F)	Ng		Np	Oil	
		lb.ft	psig		RPM	%	RPM	Pressure, psig	Temp. °C (°F)
Takeoff and Maximum/Enroute continued emergency	550	1315	42.5	750 (1380)	38,100	101.5	2200 (100%)	65-85	10 to 99 (50 to 210)
Maximum climb	538	1315	42.5	725 (1337)			2200 (100%)	65-85	0 to 99 (32 to 210)
Maximum cruise	495	1315	42.5	705 (1300)			2200 (100%)	65-85	0 to 99 (32 to 210)
Idle				685 (1265)	19,000	51.0		40 (min)	-40 to 99 (-40 to 210)
Starting				1090 (1994)					-40 (min)
Acceleration		1500	48.5	850 (1562)	38,500	102.6	2410 (110%)		0 to 99 (32 to 210)
Maximum Reverse	500	1315	42.5	750 (1380)	38,100	101.5	2090 (95%) 1960 (89%)	65-85	0 to 99 (32 to 210)

Table A.4 Control Hardware

Component	Manufacturer	Model Number
Pneumatically Actuated Ball Valves (Main fuel and purge lines)	Swagelok	SS-65CS16-33O and -33C
Pneumatically Actuated Ball Valves (Fuel manifold to engine)	Swagelok	SS-63TS8-33C
Pressure Gauges	Swagelok	p_:)
Pressure Transducers	Swagelok	PTI-E-NG3000
Check Valves	Swagelok	SS-CHS16-1
Pressure Relief Valve	Swagelok	SS-RL3S4
Solenoid Valves (pneumatic ball valve control)	Swagelok	CPN-A-SVMF4-C12D
Electronic Regulator	Tescom	ER3100SI-1
Pressure Regulator	Tescom	44-4012E208ER042
Dome Loaded Regulator	Grove	Mity-Mite Model 90
Hydrogen Meter	Omega	FTB-935
Linear potentiometer	Maurey Instrument	M3078-4-803
Uninterruptible Power Supply (UPS)	APC	BR1500LCD
Electronic Regulator Power Supply	Phoenix Contact	QUINT-PS-100-240AC/24DC/5
RS232/485 Converter	Sintech	STM485S
cDAQ module	National Instruments	NI-9472
cDAQ chassis	National Instruments	NI cDAQ-9172
Toggle switches (SPDT)	Newark	10M5078
Toggle switches (SPST)	RadioShack	275-602

Calculations for changes in shaft speed

From compressor map:

$$\frac{P_{03}}{P_{02}}, \frac{\dot{m}_a\sqrt{T_{02}}}{P_{02}}, \eta_c$$

From turbine map:

$$\frac{P_{04}}{P_{05}}, \frac{\dot{m}_{a+f}\sqrt{T_{04}}}{P_{04}}$$

Assume:

$$\frac{P_{04}}{P_{03}} \approx constant$$

Solve for T_{02}, T_{03}, T_{04}:

$$T_{02} = T_{atm}\left(1 + \frac{\gamma-1}{\gamma}M^2\right)$$

$$T_{03} = T_{02}\left(1 + \frac{1}{\eta_c}\left[\left(\frac{P_{03}}{P_{02}}\right)^{\frac{\gamma_c-1}{\gamma_c}} - 1\right]\right)$$

$$\sqrt{\frac{T_{04}}{T_{02}}} = \left[\frac{\dot{m}_a\sqrt{T_{04}}}{P_{04}}\left(\frac{P_{03}}{P_{02}}\right)\left(\frac{P_{04}}{P_{03}}\right)\right] \Big/ \frac{\dot{m}_a\sqrt{T_{02}}}{P_{02}}$$

$$T_{04} = T_{02}\left\{\left[\frac{\dot{m}_a\sqrt{T_{04}}}{P_{04}}\left(\frac{P_{03}}{P_{02}}\right)\left(\frac{P_{04}}{P_{03}}\right)\right] \Big/ \frac{\dot{m}_a\sqrt{T_{02}}}{P_{02}}\right\}^2$$

Fuel-air ratio used to calculate fuel flow:

$$f = \frac{\frac{T_{04}}{T_{03}} - 1}{\frac{Q_R}{c_p T_{03}} - \frac{T_{04}}{T_{03}}}$$

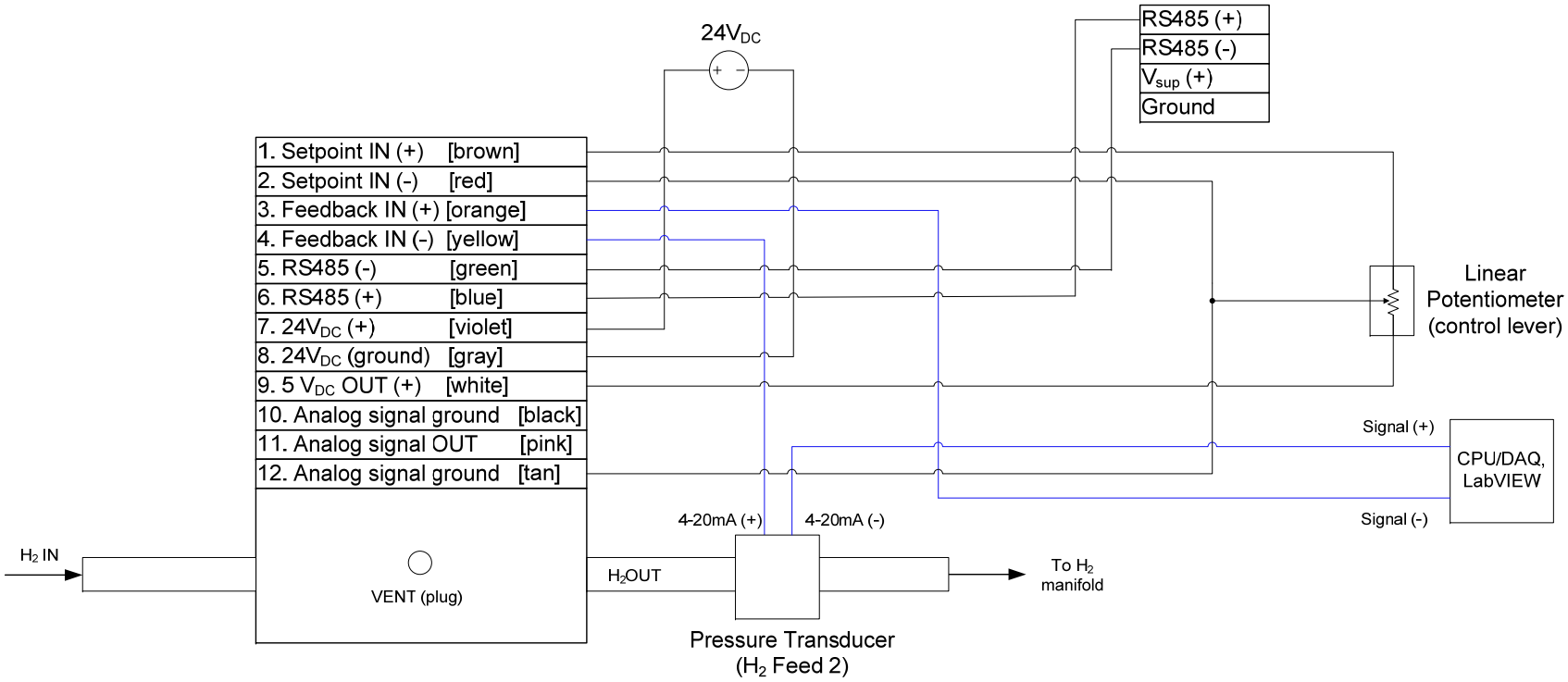

Figure A.1 ER3100 Wiring Diagram